Novel Signal Processing Approaches for Cortico-Cortical Evoked Potentials from Stereo-Electroencephalography to Improve Seizure Onset Zone Localization in Drug-Resistant Epilepsy

by

Nayereh FallahBagheri

A Dissertation Submitted to the
Graduate School of Sciences and Engineering
in Partial Fulfillment of the Requirements for
the Degree of

Master of Science
in
Biomedical Science and Engineering

KOÇ ÜNİVERSİTESİ

October 27, 2025

Novel Signal Processing Approaches for Cortico-Cortical Evoked Potentials from Stero-Electroencephalography to Improve Seizure Onset Zone Localization in Drug-Resistant Epilepsy

Koç University

Graduate School of Sciences and Engineering

This is to certify that I have examined this copy of a master's thesis by

Nayereh FallahBagheri

and have found that it is complete and satisfactory in all respects,
and that any and all revisions required by the final
examining committee have been made.

Committee Members:

_____

Prof. Dr. Sacit Karamürsel

_____

Assist. Prof. Beren Semiz Gürsoy

_____

Prof. Dr. Tamer Demiralp

_____

Prof. Dr. Sedat Nizamoğlu

Date: _____

To my parents, whose endless love, sacrifice, and encouragement have been the foundation of everything I have achieved, and to my sister, whose presence has always been a source of strength and comfort—I am forever grateful. To my dear student, Kaan Müminoğlu, whose pure heart and joy have been a source of inspiration to me, and whose presence reminded me of the beauty of learning and perseverance even in difficult times. To my advisors, Prof. Dr. Sacit Karamürsel and Assist. Prof. Beren Semiz Gürsoy, whose invaluable guidance, patience, and belief in me made this journey possible—thank you for opening the path to success. And to my dear friend, Dünya Moradi, whose unwavering support and motivation have carried me through the most challenging moments—I owe you a gratitude beyond words.

ABSTRACT

Novel Signal Processing Approaches for Cortico-Cortical Evoked Potentials from Stereo-Electroencephalography to Improve Seizure Onset Zone Localization in Drug-Resistant Epilepsy

Nayereh FallahBagheri

Master of Biomedical Science and Engineering

October 27, 2025

Drug-resistant epilepsy (DRE) remains a major clinical challenge, with many patients continuing to experience seizures despite advances in surgical interventions. Accurate delineation of the seizure onset zone (SOZ) is essential for optimizing surgical outcomes, yet current methods relying on electroencephalography, imaging, and invasive recordings are often limited by network-level complexity and inter-patient variability. Cortico-cortical evoked potentials (CCEPs) derived from stereo-electroencephalography (SEEG) provide valuable insights into brain connectivity and have been investigated as potential markers of epileptogenic tissue. Traditional analyses have focused on early and late negative deflections (N1/N2), but these components suffer from limited sensitivity, specificity, and generalizability across patients and cortical regions. In this study, we propose an advanced signal processing framework that moves beyond fixed windows and simple peak amplitudes. By extracting a broader set of features—including energy, line length, entropy, and Root Mean Square metrics—we aim to more reliably distinguish epileptogenic from non-epileptogenic regions. This approach emphasizes individualized, data-driven characterization of evoked responses to refine surgical planning. Ultimately, our framework seeks to reduce unnecessary resections, improve precision in SOZ localization, and enhance outcomes for patients with DRE.

ÖZETÇE

İlaçlara Dirençli Epilepside Nöbet Başlangıç Bölgesinin Lokalizasyonunu İyileştirmek İçin Stereo-Elektroensefalografiden Elde Edilen Kortiko-Kortikal Uyarılmış Potansiyellerde Yeni Sinyal İşleme Yaklaşımları

Nayereh FallahBagheri

Biyomedikal Bilim ve Mühendislik, Yüksek Lisans

Ekim 27, 2025

İlaçlara dirençli epilepsi (DRE), cerrahi müdahalelerdeki ilerlemelere rağmen birçok hastanın nöbet geçirmeye devam etmesiyle önemli bir klinik zorluk olmaya devam etmektedir. Nöbet başlangıç bölgesinin (SOZ) doğru bir şekilde belirlenmesi, cerrahi sonuçların optimize edilmesi açısından hayati öneme sahiptir; ancak elektroensefalografi, görüntüleme ve invaziv kayıtlar gibi mevcut yöntemler, ağ düzeyindeki karmaşıklık ve hastalar arası değişkenlik nedeniyle sıklıkla sınırlı kalmaktadır. Stereo-elektroensefalografi (SEEG) kaynaklı kortiko-kortikal uyarılmış potansiyeller (CCEP'ler), beyin bağlantısına dair değerli bilgiler sunmakta ve epileptojenik dokunun potansiyel belirteçleri olarak araştırılmaktadır. Geleneksel analizler, erken ve geç negatif dalgalanmalara (N1/N2) odaklanmıştır; ancak bu bileşenler, duyarlılık, özgüllük ve hastalar ile kortikal bölgeler arasında genellenebilirlik açısından sınırlamalara sahiptir. Bu çalışmada, sabit zaman pencereleri ve basit tepe genliklerinin ötesine geçen gelişmiş bir sinyal işleme çerçevesi öneriyoruz. Enerji, hat uzunluğu, entropi ve Kök Ortalama Kare gibi daha geniş bir özellik kümesi çıkararak epileptojenik ve epileptojenik olmayan bölgeleri daha güvenilir şekilde ayırt etmeyi amaçlıyoruz. Bu yaklaşım, cerrahi planlamayı geliştirmek için uyarılmış tepkilerin bireyselleştirilmiş, veriye dayalı karakterizasyonuna vurgu yapmaktadır. Sonuç olarak, önerilen çerçevemiz gereksiz rezeksiyonları azaltmayı, SOZ lokalizasyonunda hassasiyeti artırmayı ve DRE hastaları için sonuçları iyileştirmeyi hedeflemektedir.

ACKNOWLEDGMENTS

This study was supported by TÜBİTAK (Project No: 123S085) and TUSEB (Project No: B-22405). I would like to sincerely thank Prof. Dr. Candan Gürses (Neurology Dept.), Prof. Dr. Göktuğ Akyoldaş, and Assoc. Prof. Dr. Oğuz Baran (Neurosurgery Dept.) for kindly providing the clinical data used in this work, as well as for their valuable guidance and support throughout the study.

TABLE OF CONTENTS

LIST OF TABLES

LIST OF FIGURES

ABBREVIATIONS

DRE	Drug-Resistant Epilepsy
SOZ	Seizure Onset Zone
iEEG	intracranial Electroencephalograph
SEEG	Stereo-Electroencephalography
CCEP	Cortico-Cortical Evoked Potential(s)
LL	Line Length
PSD	Power Spectral Density
CV	coefficient of variation
SE	Spectral Entropy
RMS	Root Mean Square
RTPO	Right Temporal Parietal-Occipital
RPO	Right Parietal-Occipital
LHIP	Left Hippocampus
ROF	Right Orbitofrontal
LOF	Left Orbitofrontal
TPO	Temporo-Parieto-Occipital
HFO	High-Frequency Oscillation

CHAPTER 1

INTRODUCTION

Drug-resistant epilepsy (DRE) affects approximately one-third of patients with epilepsy, representing a major source of neurological disability and reduced quality of life (Wiebe et al., 2001). For these patients, resective surgery remains one of the most effective treatment options, with the potential to achieve long-term seizure freedom. However, despite advances in imaging, neurophysiology, and surgical techniques, surgical outcomes remain suboptimal, with a substantial proportion of patients continuing to experience seizures after resection (Jobst and Cascino, 2015). Accordingly, it is crucial to accurately map and characterize the seizure onset zone (SOZ), which plays a fundamental role in generating seizures. Identifying the SOZ is challenging, as seizures often arise from distributed networks rather than a single focus (Engel et al., 2013). Surgeons must therefore rely on multiple converging modalities, including scalp and intracranial Electroencephalography (iEEG), structural and functional imaging, and stimulation studies, to infer the boundaries of the epileptogenic tissue. Even with invasive techniques such as stereo-electroencephalography (SEEG) (Bartolomei et al., 2017), precise localization of the epileptogenic zone remains challenging. SEEG is widely used in the presurgical evaluation of patients with refractory focal epilepsy to refine SOZ boundaries and guide surgical decision-making (Rosenow and Lüders, 2001). The method allows for targeted intracranial stimulation, contributing to the precise Specification of the surgical resection zone (Jobst et al., 2020). An additional advantage of SEEG is its ability to record responses to direct electrical stimulation, giving rise to cortico-cortical evoked potentials (CCEPs)

(Matsumoto et al., 2007). As illustrated in Figure 1.1, CCEPs are brain signals generated by applying direct electrical stimulation to one cortical area and recording the response in another, offering a way to study functional connectivity and communication networks across different brain regions (Al-Sadek et al., 2025). The application of CCEPs has facilitated the mapping of multiple cortical networks implicated in language (Matsumoto et al., 2004, 2007), limbic (Enatsu et al., 2015), motor (Matsumoto et al., 2007), auditory (Howard et al., 2000), and visual systems (Huang et al., 2023). CCEPs serve an important clinical role in intraoperative mapping, helping to protect vital functional areas during epilepsy and tumor surgeries (Saito et al., 2014; Mariani et al., 2021; Seidel et al., 2024). They have also been applied to identify SOZ (van't Klooster et al., 2011) and biomarkers of epileptogenicity (Mouthaan et al., 2016). Classically, CCEPs are described as comprising two main components: an early negative deflection at 10–30 ms (N1) and a slower wave at 80–250 ms (N2) (Lemaréchal et al., 2022; Kunieda et al., 2015; Keller et al., 2014). More recently, some groups have shifted toward labeling early and late deflections as D1/D2 (Feys et al., 2025; Alarcón et al., 2018), but such simplifications risk overlooking patient- or region-specific variability, atypical responses, or later emerging components (Al-Sadek et al., 2025).

Both N1 and N2 have interpretive challenges. N1 is often taken as a proxy of monosynaptic cortico-cortical connectivity, yet latency or amplitude alone may not reliably distinguish epileptogenic from non-epileptogenic tissue (Tomlinson et al., 2025). N2, meanwhile, reflects more complex polysynaptic or subcortico-cortical activity, making its significance for SOZ detection less clear. In fact, electrodes within the SOZ frequently show attenuated amplitudes of N1 / N2 compared to non-SOZ sites (Cornblath et al., 2023), however, variability between patients and brain regions restricts broad applicability.

Recent studies highlight both the promise and the drawbacks of relying on N1/N2. For example, Root mean square (RMS)-standardized N1/N2 measures from SEEG-based CCEPs have been incorporated into support vector machine models predicting surgical outcomes in temporal lobe epilepsy, showing that strong connectivity involving unresected SOZ regions predicts poorer outcome (Hu et al., 2025). Yet these models still empha-

size peak amplitudes within fixed windows, neglecting waveform morphology, trial-level variability, and later components. Although larger N1 amplitudes are often associated with SOZ stimulation, the results remain inconsistent between patients. More advanced approaches—including deep learning, time–frequency analysis, and connectivity metrics—offer richer information but remain retrospective, computationally demanding, and unvalidated in prospective trials (Tomlinson et al., 2025).

Overall, N1 and N2 remain useful, accessible markers, but their limited sensitivity, specificity, and generalizability mean that "strong" N1/N2 responses cannot serve as definitive indicators of epileptogenicity. Fixed detection windows also risk missing variable or attenuated responses (Cornblath et al., 2023; Qiang et al., 2025).

In this study, we first analysed the N1/N2 peaks on our data sets, after realizing the limitations of this approach, we move beyond fixed windows and simple peak-based analyses. Using SEEG-derived CCEPs data, we applied advanced signal processing methods to extract richer features, including Shannon entropy, spectral entropy (SE), energy and line length (LL), along with Root Mean Square (RMS) analyzes. These approaches aim to capture both local and distributed activations, improving the identification of epileptogenic regions. Ultimately, this framework seeks to reduce surgical extent while offering more reliable, individualized markers of epileptogenic tissue in DRE.

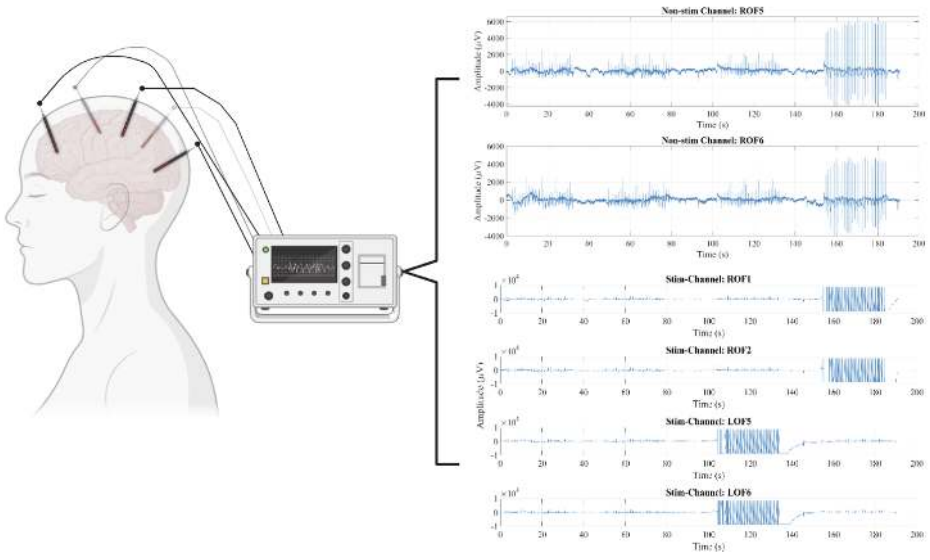

Figure 1.1. An illustration of the CCEPs driven from SEEG data.

CHAPTER 2

METHODOLOGY

In this section, the methodological steps undertaken for the analysis of CCEPs are described in detail. The procedure consists of four main steps: (i) data acquisition, (ii) signal preprocessing, (iii) feature extraction, and (iv) RMS analysis, aimed at identifying SOZ candidates. The overall workflow is summarized in the flowchart below (see Figure 2.1), followed by a step-by-step explanation of each component.

Figure 2.1. Workflow of the proposed methodology.

2.1 *Data Acquisition*

In this study, SEEG data were collected from 12 patients with focal epilepsy (7 females, 5 males; age range: 15–37 years) who underwent invasive monitoring at Koç University Hospital. All patients were implanted with intracranial electrodes, with the number of implanted channels ranging from 48 to 120. Electrode placement was determined by the clinical team according to the suspected seizure onset zones and propagation pathways of each patient.

Electrical stimulation was delivered in a pairwise manner across selected electrode contacts for 30 seconds at 1 Hz. The number of stimulated channels varied between 4 and 12.

Stimulation intensity ranged from 3 to 15 mA: most patients received a fixed intensity of either 10 mA (6 patients) or 15 mA (5 patients), while one patient received stimulation at different intensities (3, 5, and 10 mA) applied to different channels.

All recordings were acquired in European Data Format (EDF) with a sampling frequency of 2048 Hz, providing high temporal resolution for subsequent analyses. A complete summary of patient demographics, number of total electrode's channels, and stimulation parameters is provided in Table 2.1. No additional preprocessing was applied during acquisition beyond standard clinical monitoring procedures.

Channel Selection

Since the data are subject-specific, each patient had unique electrode implantation sites and therefore individualized channel labels. To account for this variability, the analysis pipeline was designed so that the stimulated channels are explicitly defined for each patient (see Algorithm 1). This approach ensures that analyses are performed on the correct set of channels. Following this step, the channels for each patient were systematically divided into two groups: (i) stimulated channels and (ii) non-stimulated channels.

Table 2.1. Summary of patient demographics and acquisition parameters.

Patient ID	Sex	Age	No. of Channels	No. of Stimulated Channels	Stim. Intensity (mA)
1	M	31	64	6	10
2	M	37	48	12	3, 10, 5
3	F	24	78	12	15
4	M	20	48	4	10
5	F	24	76	10	10
6	M	17	66	6	10
7	F	36	48	10	10
8	M	25	76	8	15
9	F	15	72	8	10
10	F	26	80	10	15
11	F	23	112	10	15
12	F	16	120	8	15

Algorithm 1 Data Acquisition

1: Read EDF file → `data`
2: Extract channel names → `ch_names`
3: Define stimulated channels manually for each patient: {`insert patient-specific channel names`}
4: Keep only existing stim channels in EDF
5: **if** no valid stim channels **then**
6: **error**
7: **end if**
8: Non-stim channels ← remaining in `ch_names`
9: **if** no valid non-stim channels **then**
10: **error**
11: **end if**
12: n_{stim} ← count(stim channels)
13: n_{total} ← count(all channels)

2.2 *Signal Preprocessing*

Following data acquisition, the recordings were preprocessed to remove noise and stimulation-related artifacts, ensuring cleaner signals for subsequent analyses. The preprocessing pipeline consisted of two main stages: Signal filtering and noise removal, artifact detection and inpainting.

Signal Filtering: The first step involved cleaning the signals to remove physiological and power-line noise, followed by interpolation (Xie et al., 2023; Wang et al., 2024). Each channel was processed using a fourth-order Butterworth bandpass filter (1–1000 Hz) and a 50 Hz notch filter to ensure signal fidelity and suppress residual distortions. The fourth-order design was selected for its steeper roll-off (24 dB/octave), which provides effective attenuation of out-of-band noise while preserving neural activity up to 1 kHz, consistent with established iEEG preprocessing practices (Schaworonkow and Voytek, 2021; Akkol et al., 2021). Power-line interference was further mitigated using the 50 Hz notch filter, following standard SEEG/iEEG signal processing protocols (Widmann et al., 2015). This combined filtering procedure ensured that the resulting non-stimulated channel signals were artifact-free, physiologically meaningful, and spectrally consistent across recordings.

Artifact detection and inpainting: Since electrical stimulation induces strong transient

artifacts in the recorded signals, a dedicated cleaning procedure was applied to the non-stimulated channels. First, a 30-second sliding window was employed to identify the highest-energy epoch in the stimulated channels. The corresponding time window in the non-stimulated channels, containing exactly 30 stimulation events, was then selected. Using derivative-based peak detection with a dynamic threshold, each stimulation peak was identified, and a ±10 ms interval around it was marked as artifact-contaminated. These contaminated segments were then removed and reconstructed using a two-step interpolation procedure: linear interpolation to maintain a smooth temporal evolution of the signal, followed by nearest-neighbor interpolation to fill any remaining gaps (see Figure 2.3).

Algorithm 2 Artifact Removal in Non-Stimulated Channels

```
Apply 4th-order Butterworth bandpass and 50 Hz notch filter to all the channels
for each stimulated channel do
    Compute signal derivative
    Apply a sliding 30-second window across the recording
    Detect the 30 sec epoch with maximum energy
    Find the corresponding 30-second epoch in non-stim channels
    Find stimulation peaks using derivative and dynamic threshold
    Mark ±10 ms around each detected peak as artifact
    Inpaint artifacts using linear interpolation, then nearest-neighbor filling
    Store the cleaned channel signal
end for
```

As outlined in Algorithm 2, a 30-second sliding window was applied to the stimulated channels to identify the epoch with the highest energy. This window corresponds to the stimulation period, which consistently exhibits maximal energy across recordings (see Figure 2.2).

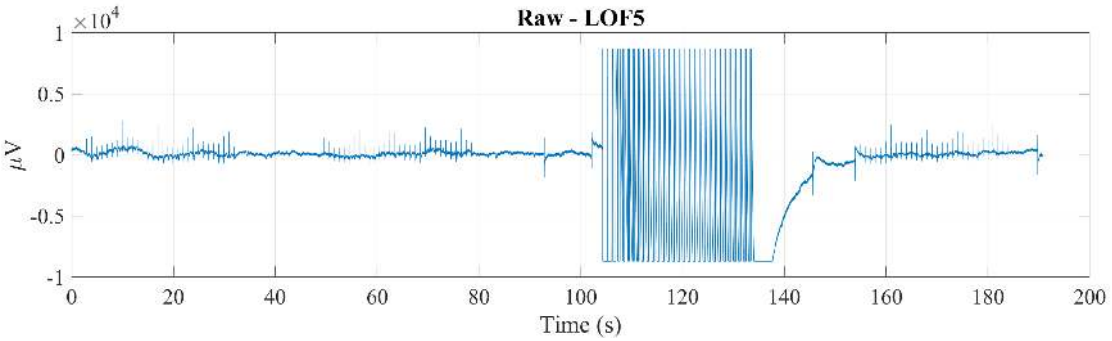

Figure 2.2. A sample of a full recording of one stimulated channel.

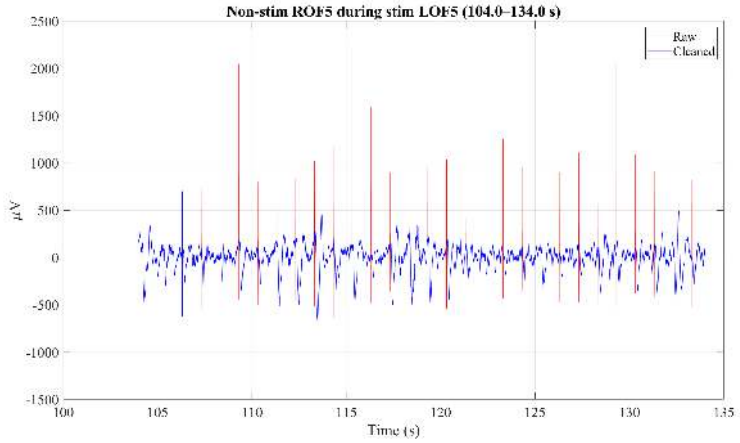

(a)

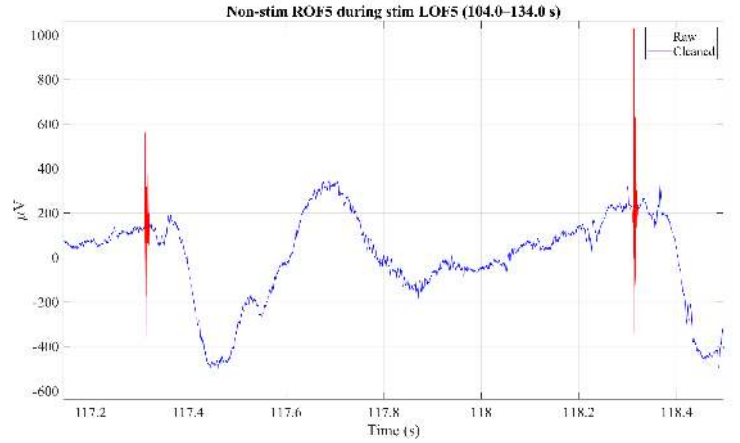

(b)

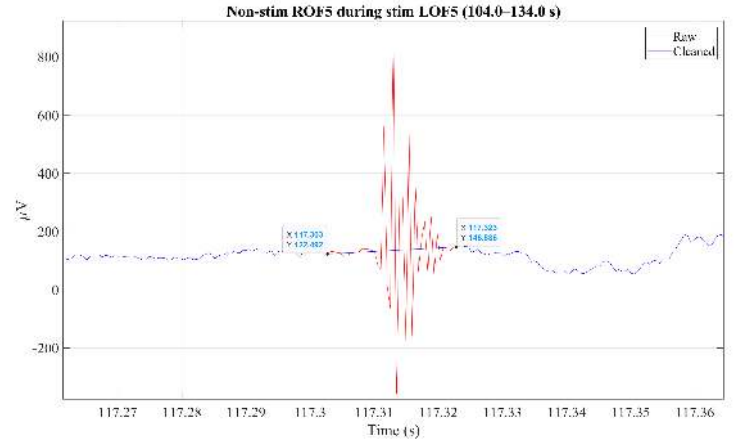

(c) Third subfigure

Figure 2.3. Illustration of the raw signal from a non-stimulated channel (ROF5) and its filtered, artifact-free version obtained through interpolation, aligned with the selected stimulated channel. (a) Full 30-s epoch. (b) Example of two consecutive artifact removals. (c) Close-up view of the interpolation process.

2.3 *Feature Extraction* (*Non-stimulated Channels*)

Feature extraction was performed on the set of non-stimulated channels to characterize neural dynamics and identify candidate SOZs. The process consisted of four stages: Epoching, windowing and entropy measures, additional temporal feature extraction and aggregation into a SOZ score.

2.3.1 Epoching:

At this stage, the filtered non-stimulated channels were used prior to artifact removal. The signals were then divided into 30-second epochs with a 1-second hop size within an analysis window of up to 200 seconds, depending on the available signal length. This overlapping segmentation ensured dense temporal coverage and provided multiple candidate segments for feature evaluation.

Two features—signal energy and LL—were computed for each epoch. Signal energy captures periods of heightened neural activity, as seizures are typically associated with elevated power, while LL reflects temporal complexity and rapid fluctuations in the signal. Previous studies have demonstrated that both features exhibit strong discriminative power for distinguishing seizure-related from baseline activity (Boonyakitanont et al., 2020; Kharbouch et al., 2011).

Accordingly, feature extraction was performed on epochs with the highest energy and LL values, as these segments are most likely to contain structured neural activity and provide the most informative signal characteristics. As described in Algorithm 3, both features were computed for each 30-second epoch in the non-stimulated channels. Because high energy typically corresponds to high-amplitude activity, it was essential to ensure that the selected 30-second epoch reflected the stimulation period, which should contain approximately 30 evoked responses (peaks). To account for inter-channel variability and avoid discarding valid epochs, this criterion was relaxed to require at least 25 peaks. Thus, the epoch with the highest energy was selected if it contained at least 25 peaks, indicating responsiveness of that channel; otherwise, the epoch with the highest LL was chosen. This

procedure ensured that the selected epoch either captured strong stimulus-related activity (via energy) or retained the most temporally complex segment (via LL) when the energy criterion was not met.

Algorithm 3 Epoch Selection Based on Energy and Line Length

for each non-stim channel **do**
  Select first 200 seconds of signal
  Divide signal into 30-sec epochs with 1-sec step
  for each epoch **do**
    Compute $Energy = \sum epoch^2$
    Compute $LL = \sum |\Delta epoch|$
  end for
  $idx\_energy \leftarrow$ index of epoch with maximum Energy
  $idx\_LL \leftarrow$ index of epoch with maximum Line Length
  $best\_energy\_epoch \leftarrow$ epoch at idx_energy
  $best\_LL\_epoch \leftarrow$ epoch at idx_LL
  Find peaks in $best\_energy\_epoch$ with:
   prominence $\geq std(best\_energy\_epoch)$
   min peak distance = 1800 samples
  Keep only peaks $\geq$ 1000 amplitude
  if number of peaks $\geq$ 25 **then**
    $selected\_epoch \leftarrow best\_energy\_epoch$
    $epoch\_type \leftarrow$ "energy"
    $best\_epoch\_idx \leftarrow idx\_energy$
  else
    $selected\_epoch \leftarrow best\_LL\_epoch$
    $epoch\_type \leftarrow$ "line length"
    $best\_epoch\_idx \leftarrow idx\_LL$
  end if
  Use $selected\_epoch$ for feature extraction
end for

2.3.2 Windowing and Entropy Measures:

After identifying the most responsive 30-second epoch from each non-stimulated channel (see Figure 2.4a), the signal was further divided into 30 consecutive analysis windows. Each window spanned one second in duration (see Figure 2.4b); however, only the central 0.98 seconds were retained for feature computation. The initial 0.02 seconds were intentionally discarded in order to minimize potential interference from stimulus-related artifacts. Empirical observations confirmed that stimulus artifacts on non-stimulated chan-

nels typically persisted for approximately 0.02 seconds (see Figure 2.4c). Within each of these windows, two complementary entropy measures were computed: *Shannon Entropy* and *SE*.

- *Shannon Entropy:* Estimated from the amplitude probability distribution of the signal, quantifying the degree of uncertainty or randomness in the time-domain amplitude values (Lo et al., 2022). For each analysis window, the signal amplitudes were histogrammed into N bins and normalized to obtain a discrete probability distribution g_i over the bins. The Shannon entropy was then computed as below (Shannon, 1948).

$$H_{\text{Shannon}} = -\sum_{i=1}^{N} g_i \log_2(g_i).$$

  Where g_i represents the probability of the i-th bin and terms with $g_i = 0$ are excluded. This formulation captures how spread or concentrated the amplitude distribution is: higher values correspond to greater randomness, whereas lower values indicate more structured or deterministic signal behavior.

- *Spectral Entropy:* Estimated from the normalized power spectral density (PSD) using Welch's method, SE has been shown to capture both electrophysiological and physiological alterations in DRE (Helakari et al., 2019). As a scale-free measure, SE provides a robust and comparable metric that has also been demonstrated to reflect epileptic pathology in intracranial recordings (Aarabi et al., 2009). Conceptually, SE quantifies the distributional complexity of the signal in the frequency domain by assessing how evenly or unevenly spectral power is distributed across frequencies (Tenev et al., 2025). In our analysis, Welch's method was selected over a direct fast Fourier transform (FFT) because it yields more reliable PSD estimates for SEEG data, which are characteristically noisy and non-stationary. Specifically, Welch's approach divides the signal into overlapping segments, applies windowing functions to reduce spectral leakage, and averages the resulting periodograms (Welch, 1967). This procedure decreases the variance of the spectral estimates and enhances ro-

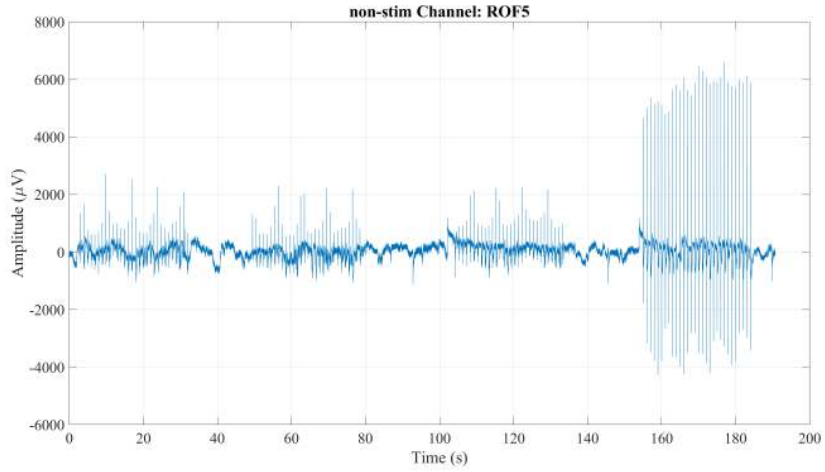

(a)

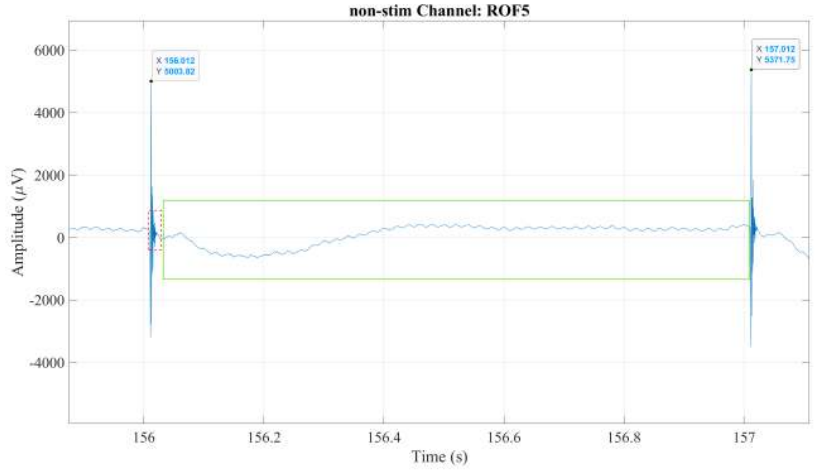

(b)

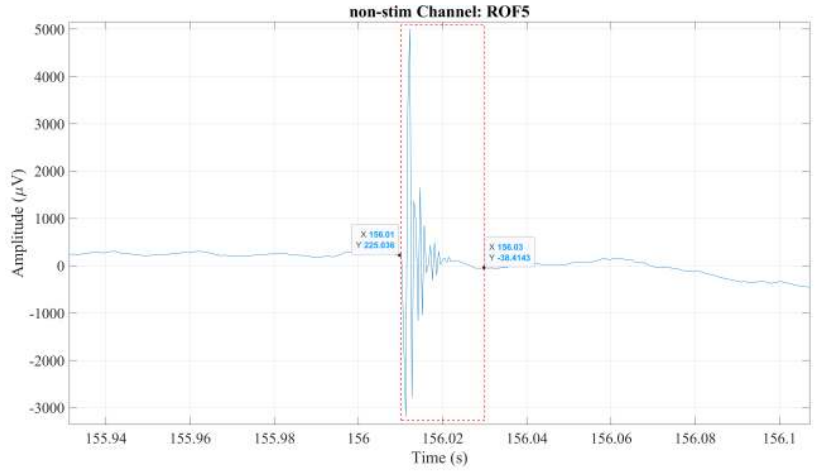

(c)

Figure 2.4. Illustration of a typical non-stimulated channel and the analysis time windows. (a) Full raw data. (b) A one-second analysis segment. (c) Duration of observed stimulus artifact.

bustness against transient fluctuations, thereby ensuring that the computed entropy values reflect the underlying spectral structure of the signal rather than noise or stimulation-driven artifacts.

The PSD obtained through Welch's method was then normalized to form a probability distribution, which served as the basis for SE computation. Mathematically, SE is defined as follows (Inouye et al., 1991):

$$H_{\text{spectral}} = -\sum_{i=1}^{N} P(f_i)\ \log_2\left(P(f_i)\right).$$

Where $P(f_i)$ denotes the normalized power spectral density at frequency bin f_i, such that $\sum_{i=1}^{N} P(f_i) = 1$. A higher entropy indicates that spectral power is more evenly distributed across frequencies, whereas lower entropy reflects concentration of power within a narrower frequency range (Tian et al., 2017). In the context of CCEPs, SE provides a concise measure of how the evoked response distributes its power across the frequency spectrum: lower values indicate narrowband, synchronized oscillatory activity characteristic of pathological or epileptogenic networks, whereas higher values correspond to broadband, desynchronized activity more typical of physiologically normal responses. To the best of our knowledge, the application of SE to the analysis of CCEPs responses in SEEG recordings has not been previously reported, and therefore represents a novel methodological contribution of this work.

In addition to the mean values, the coefficient of variation (CV) of each entropy measure was also included to capture the temporal dynamics of the signal within the 30-second epoch. While the mean entropy provides a global summary of the average information content, it does not account for potential fluctuations in entropy across successive windows. The coefficient of variation (CV = standard deviation / mean), offers a normalized measure of variability that is independent of the absolute magnitude of the entropy values (Angulo-Ruiz et al., 2023). In the context of SEEG and CCEPs analysis, a higher CV reflects greater instability or non-stationarity of the neural response, potentially indicating transient bursts of synchrony or irregularity that may be masked when only mean values are considered.

Conversely, a lower CV suggests more consistent and stable information content throughout the epoch. By combining both mean and CV, the analysis captures not only the central tendency of the entropy but also the degree of temporal variability, thereby providing a more comprehensive characterization of the electrophysiological dynamics. This dual representation is particularly valuable in epilepsy research, where pathological networks often exhibit both abnormal baseline entropy levels and atypical variability across time.

2.3.3 Additional Temporal Feature Extraction

In addition to the entropy-based measures described above, two complementary temporal features were extracted from the selected 30-second epoch as a whole. Unlike entropy, which was estimated on short sub-windows to capture fluctuations in information content, these features were intentionally computed over the entire epoch. This decision was motivated both by their mathematical properties and by the need to obtain stable, representative descriptors of neural activity.

Specifically, signal energy and LL are inherently additive quantities. Energy, defined as the sum of squared amplitudes (Singh and Krishnan, 2023), and LL, calculated as the cumulative absolute difference across adjacent samples (Ye et al., 2022), both scale naturally with signal duration. Computing these features on shorter windows and averaging the results would yield values highly correlated with the single-epoch calculation, thereby introducing redundancy without adding interpretive value.

In summary, entropy measures were evaluated on 0.98-second sub-windows to capture both mean values and temporal variability via CV, whereas energy and line length were calculated directly over the full 30-second epoch. This decision highlights a careful trade-off: entropy quantifies short-term fluctuations, while energy and line length provide concise and reliable representations of stable signal properties.

2.3.4 Normalization, SOZ Scoring, and Visualization

All extracted features were first normalized using the z-score transformation in order to place them on a common scale and to attenuate biases arising from differences in absolute

magnitude across feature types (Shoeibi et al., 2021). The z-score of a value a is defined as below (Kirch, 2008):

$$z = \frac{a - \mu}{\sigma}.$$

Where μ and σ denote the mean and standard deviation of that feature across all channels, respectively. This transformation shifts the distribution of each feature to have zero mean and rescales it to unit variance (Wu et al., 2022). In practical terms, a z-score expresses how many standard deviations a given feature value of a channel lies above or below the population mean.

SOZ Scoring via Feature Averaging: Following normalization, a single SOZ score was computed for every channel by averaging its normalized feature values (Thompson, 2004) (energy, LL, Shannon entropy CV, and SE CV).

$$\text{SOZScore}(c) = \frac{1}{N} \sum_{i=1}^{N} z_{c,i}.$$

Where $z_{c,i}$ represents the z-scored value of the i-th feature for channel c, and N is the number of features (here $N = 4$). This averaging strategy serves three main purposes. First, it integrates information from complementary feature domains, combining temporal descriptors (energy, LL) with measures of spectral variability (entropy coefficients). Second, by aggregating across features, it reduces sensitivity to noise or outliers that may disproportionately affect a single metric. Finally, the SOZ score serves as a unified ranking measure, enabling identification of the channels most consistently linked to seizure onset activity.

In this way, rather than relying on any single descriptor, the methodology yields a balanced, multi-feature index of epileptogenicity that is both robust and interpretable.

Visualization: The resulting SOZ scores were visualized in two complementary ways:

1. **SOZ Heatmap:** A heatmap of z-scored feature values across all non-stimulated channels, sorted by SOZ score, providing an overview of relative feature distributions.

2. **Top-10 SOZ Channels:** A bar plot displaying the ten non-stimulated channels with the highest SOZ scores, highlighting those most likely to represent seizure onset regions.

The structured pipeline, presented in Algorithm 4, enabled a systematic and quantitative comparison of non-stimulated channels by integrating temporal and spectral features to identify candidate SOZ regions.

Algorithm 4 Feature Extraction, SOZ Scoring, and Visualization

for each channel c in desired channels **do**
    Load raw signal x_c
    Apply band pass and notch filtering
    Limit to first 200 seconds of data
    Segment into 30-second epochs with 1-second hop
    for each epoch **do**
        Compute Energy = $\sum x^2$
        Compute Line Length = $\sum |x_{i+1} - x_i|$
    end for
    Select best epoch using maximum Energy or LL
    Apply peak-based heuristic to finalize epoch
    Divide selected epoch into 0.98-second windows
    for each window **do**
        Compute Shannon Entropy
        Compute Spectral Entropy
    end for
    Compute Energy and LL on full 30-second epoch
    Store: Energy, LL, Shannon Entropy (mean, CV), Spectral Entropy (mean, CV)
end for
Normalize all features across channels using z-score
For each channel, compute SOZ Score = mean of normalized features
Rank channels by SOZ Score
Visualization:

- Heatmap of z-scored features sorted by SOZ Score
- Bar plot of Top-10 channels with highest SOZ Score

2.4 *Root Mean Square Analysis*

After extracting features from the non-stimulated channels and identifying the strongest SOZ candidates, the next step involved computing the RMS of their signals to assess the temporal network connectivity. This analysis aimed to identify regions functionally linked to the stimulated areas.

In CCEP studies, the RMS value of the averaged evoked potential has been utilized as a quantitative measure of effective connectivity. RMS values computed across insular gyri have been used to rank connection strength in sEEG recordings Dionisio et al. (2019). More recently, comparisons between RMS and amplitude measures have shown that processing choices, such as filtering and referencing, can significantly influence CCEPs quantification Levinson et al. (2024). RMS deviation from baseline is also described as one of the key methods for CCEP quantification Qiang et al. (2025). From a clinical-network perspective, higher RMS (and related amplitude metrics) have been associated with more pathologic connectivity in focal epilepsy, particularly in regions closer to the seizure-onset zone Parker et al. (2018). Finally, depth-electrode studies further confirm the utility of RMS measures in SEEG recordings and emphasize the importance of electrode montage and preprocessing in interpreting results Mitsuhashi et al. (2020).

Here, we quantified CCEPs magnitude using the RMS of the cleaned evoked epoch for each non-stimulated channel. For a time series $x(t)$ with N samples, RMS was computed as below Sanei and Chambers (2013):

$$\mathrm{RMS}(x) = \sqrt{\frac{1}{N}\sum_{t=1}^{N} x(t)^2}.$$

This measure provides a polarity-invariant, energy-like index summarizing the overall magnitude of the evoked potential across time. Unlike single-point amplitude measures, RMS integrates the entire waveform, thus reducing sensitivity to latency variability and multiphasic morphology. Higher RMS values reflect larger evoked responses and have been associated with stronger or more pathologic connectivity in focal epilepsy.

Implementation. For each stimulation index (s) and recording channel (c), the cleaned 30 s epoch (`clean_epoch`) was processed as follows:

Algorithm 5 Computation of RMS for Cleaned CCEP Epochs

1: **for** each stimulation index $s = 1$ to n_{stim} **do**
2: **for** each recording channel $c = 1$ to n_{channels} **do**
3: Extract cleaned epoch: $x \leftarrow$ `clean_epoch`(s, c) (the cleaned inpaited non-stim signals from preprocessing step)
4: Compute RMS: `RMS_clean`$[s, c] \leftarrow \sqrt{\text{mean}(x^2)}$
5: **end for**
6: **end for**
7: Exclude stimulated channels: `RMS_clean`$[:,$ `isStimCh`$] \leftarrow$ NaN

The resulting matrix `RMS_clean` had rows corresponding to stimulation sites and columns to recording contacts. Stimulated-channel columns were set to NaN to avoid contamination from local stimulation artifacts.

Visualization: The two-dimensional RMS matrix was displayed as a heatmap using a jet colormap, with axes denoting stimulated and recording channels. Color scaling was limited to the 5th–95th percentile range of non-NaN RMS values to improve contrast and minimize outlier effects.

Justification: RMS was selected as the primary quantification metric because:

- It captures the overall energy of the evoked response, independent of polarity.
- It is robust to waveform shape and latency jitter, offering a more stable comparison across trials, channels, and subjects.
- It provides a standardized, quantitative measure of effective connectivity that aligns with previous CCEP and SEEG studies.

Overall, by analyzing the RMS values of non-stimulated channels within the time window corresponding to each stimulation, we can infer functional connections between brain regions. Channels that show strong RMS responses to stimulation indicate regions that are functionally engaged within the same network.

CHAPTER 3

RESULTS AND DISCUSSION

This study aimed to localize the SOZ in patients with DRE by analyzing CCEPs obtained from SEEG recordings. In patients with DRE, resection of the epileptogenic region is required to achieve seizure control, and accurate identification of this region is crucial to minimize postoperative complications and optimize surgical outcomes.

Using invasive stimulation procedures and the corresponding patient recordings, we analyzed SEEG signals to identify potential SOZ candidates. In this section, we present the results of these analyzes, encompassing the entire workflow from feature extraction to the computation of RMS metric in our patient cohort.

3.1 *Patient* 1 *Results*

3.1.1 Connectivity Analysis Outcomes

Patient 1 (see Table 2.1) had a total of 64 channels, of which 6 were stimulated with an intensity of 10 mA, as shown in Figure 3.1. The results for this patient are presented below:

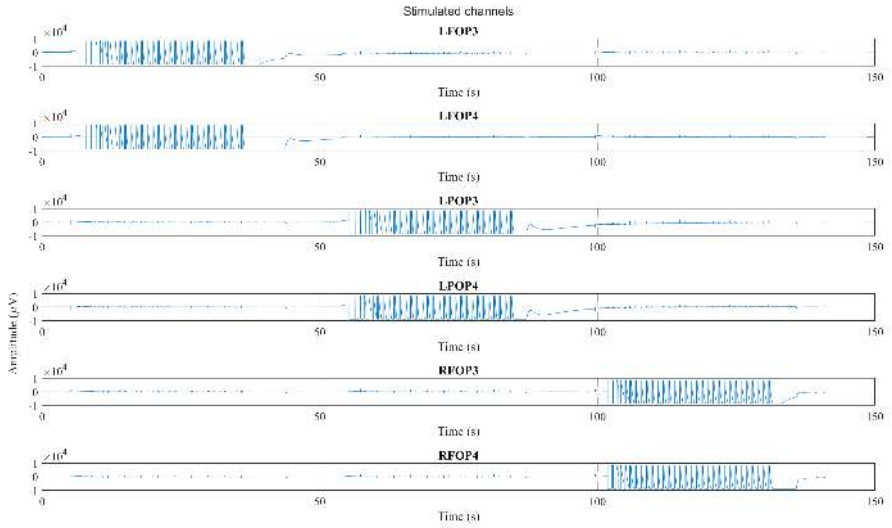

Figure 3.1. All 6 stimulated channels for patient 1.

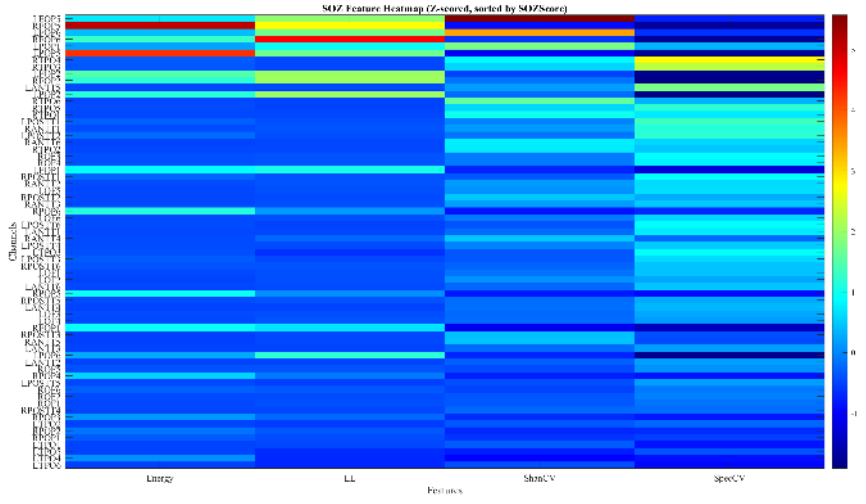

Figure 3.2. Z-score heatmap of feature extractions from non-stimulated channels in Patient 1.

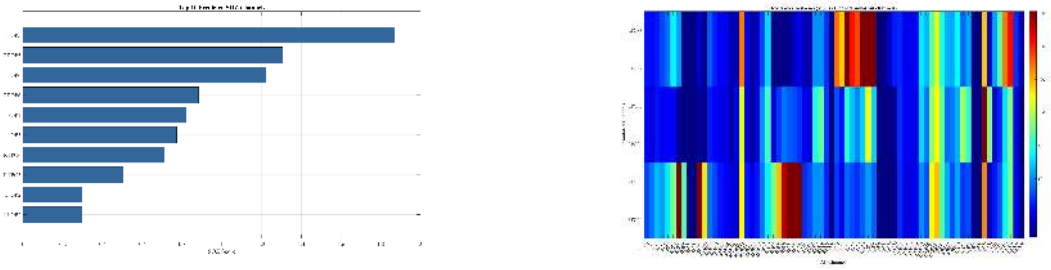

(a) **(b)**

Figure 3.3. (a) Top 10 SOZ candidate channels identified through feature extraction. (b) RMS connectivity among the regions.

3.1.2 Evaluation and Alignment of Methods

The clinical evaluation documented three seizures in this patient: two with right temporal parietal-occipital (RTPO) onset and one with right parietal-occipital (RPO) onset. Notably, during the second seizure, rhythmic activity propagated to the left hemisphere, suggesting secondary involvement beyond the primary onset region. Interictal findings further revealed multiple epileptogenic foci, consistent with a distributed and multifocal epileptic network rather than a single localized SOZ.

Signal processing analysis provided complementary insights by ranking the top 10 predicted SOZ channels based on quantitative scoring (Figure 3.3a). LFOP5, RFOP5, and LFOP6 emerged as the strongest candidates, while RTPO3 and RTPO4—clinically significant regions—were included but ranked lower. This indicates a partial divergence between the clinical findings, which emphasized right temporal onset, and computational results, which highlighted bilateral frontal–orbital contributions, with particularly strong signals from the left hemisphere.

The RMS analysis showed clear patterns of how different brain regions are connected and respond to stimulation. As seen in Figure 3.3b, stimulating the left fronto-opercular sites (LPOP3–LPOP4) mainly increased activity in nearby left-hemisphere areas, especially in the left frontal and opercular regions. This suggests strong local connections within the same hemisphere. On the other hand, stimulating the right fronto-opercular sites (RFOP3–RFOP4) produced broader responses, including in both right and left prefrontal regions. This indicates that the right hemisphere may be more involved in cross-

hemispheric communication. Some channels showed very high RMS values (above 120 μV), pointing to especially strong connections between specific regions. Overall, these results suggest that the left and right opercular areas act as important hubs in the brain's network, linking different frontal regions within and across hemispheres.

Therefore, the alignment between clinical and computational findings is partial—the analyses converge on the presence of a bilateral and distributed epileptic network, but diverge on the dominant hemisphere and specific onset territories. In other words, both approaches support a multifocal, interconnected epileptogenic system, yet the computational models emphasize frontal–opercular contributions more than the posterior temporal–parietal regions identified clinically.

3.2 *Patient 2 Results*

3.2.1 Connectivity Analysis Outcomes

Patient 2 (see Table 2.1) had a total of 48 channels, 12 of which were stimulated at intensities of 15, 10, or 3 mA, (see Figure 3.4). Among these, the electrode placed in ROPER included four stimulated channels. The results for this patient are presented below:

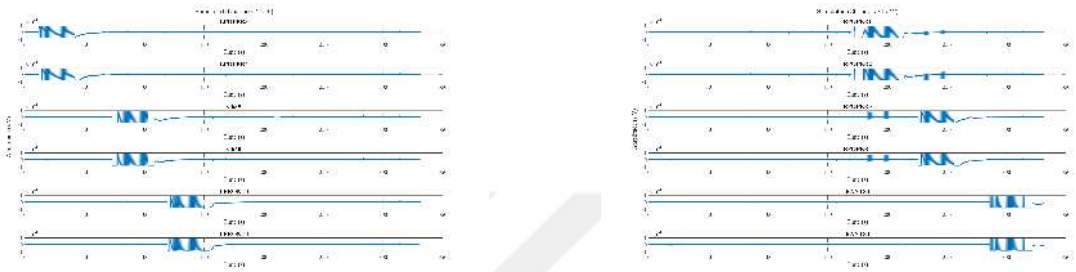

(a) **(b)**

Figure 3.4. All 12 stimulated channels in patient 2 over 350 seconds.

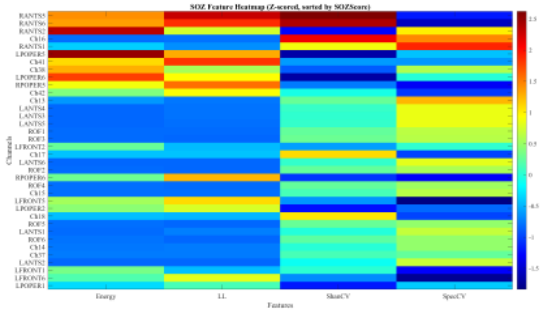

Figure 3.5. Z-score heatmap of feature extractions from non-stimulated channels in Patient 2.

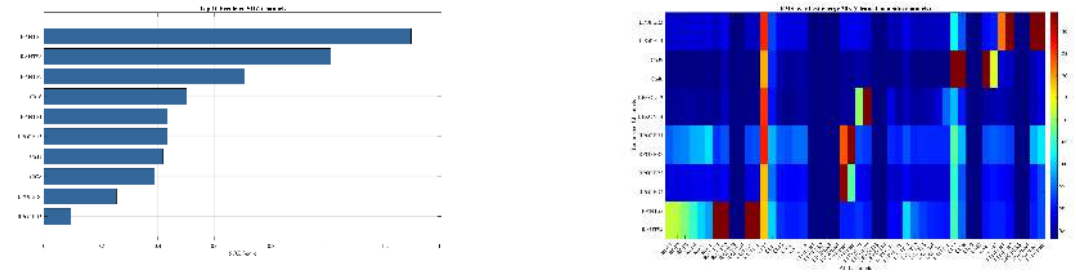

(a) **(b)**

Figure 3.6. (a) Top 10 SOZ candidate channels based on feature extraction. (b) RMS connectivity among the regions.

3.2.2 Evaluation and Alignment of Methods

The clinical evaluation for this patient established that all eight recorded seizures originated from the left dorsolateral frontal region, specifically involving electrode contacts 1–2. This localization was further supported by interictal findings, which indicated multiple epileptogenic foci concentrated in the same dorsolateral frontal area. Thus, the clinical evidence strongly points to a frontal lobe onset with lateralized activity to the left hemisphere as the dominant source of seizure generation.

The RMS analysis during stimulation revealed clear patterns of connectivity between different cortical regions. As shown in Figure 3.6b, stimulation of the left opercular (LPOPER3–LPOPER4) and left frontal (LFRONT3–LFRONT4) areas mainly produced activity in nearby left-hemisphere channels, indicating strong local connections within the frontal and opercular regions. In contrast, stimulation of right opercular (RPOPER1–RPOPER4) and right anterior temporal (RANTS3–RANTS4) channels resulted in more widespread responses, including activity in both ipsilateral and contralateral sites. This suggests that the right hemisphere may play a key role in integrating signals across hemispheres. Several high RMS values (above 120 µV) were observed in channels around central and frontal regions, pointing to strong functional coupling in those areas. Overall, the results indicate that both hemispheres contribute to a connected fronto-temporal network, with the opercular regions acting as major hubs for bilateral communication and signal propagation.

Overall, the clinical and computational findings are partially aligned. Both analyses support the left dorsolateral frontal cortex as the primary seizure onset zone, while the RMS and SOZ analyses further reveal network-level propagation extending into the right anterior temporal regions, indicating a more distributed epileptic network.

3.3 *Patient 3 Results*

3.3.1 Connectivity Analysis Outcomes

Patient 3 (Table 2.1) had a total of 78 channels, 12 of which were stimulated at an intensity of 15 mA. Four of these stimulation sites were located in the right orbitofrontal (ROF) region (see Figure 3.7). The results for this patient are presented below:

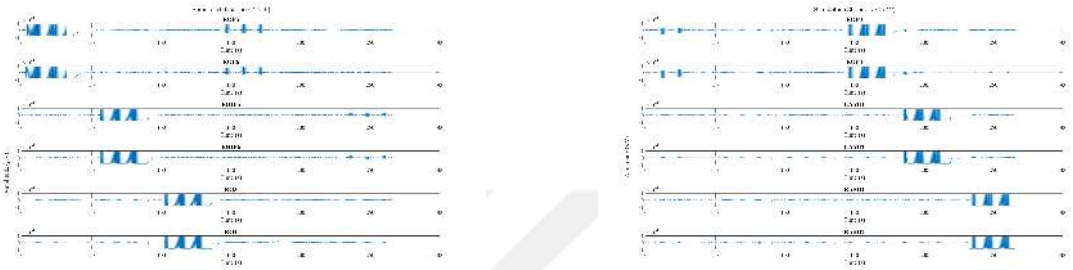

(a) **(b)**

Figure 3.7. Stimulated channels in patient 3 over 300 seconds.

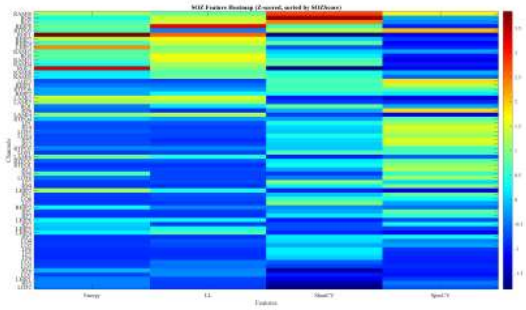

Figure 3.8. Z-score heatmap of feature extractions from non-stimulated channels in Patient 3.

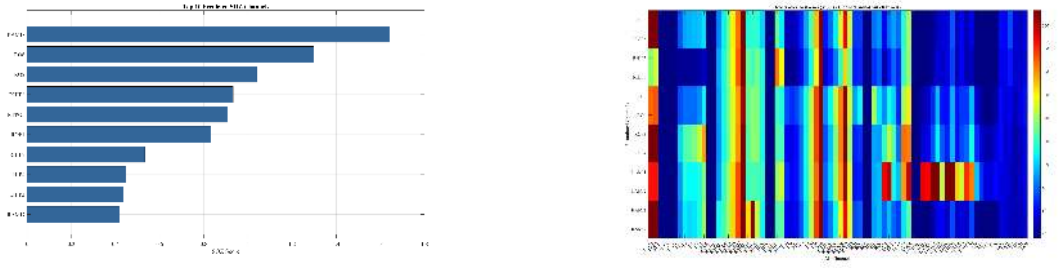

(a) **(b)**

Figure 3.9. (a) Top 10 SOZ candidate channels based on feature extraction. (b) RMS connectivity among the regions.

3.3.2 Evaluation and Alignment of Methods

The computational signal analysis identified the top predicted SOZ channels primarily within the right mesial temporal structures, including the amygdala and hippocampus (RAMI8, RO6, RO2, RHIP8, RTPO5; Shown in Figure 3.9a). This closely aligns with clinical observations, which reported that five of six seizures originated in the right hippocampus, confirming strong right-sided dominance. The clinical report also emphasized the right amygdala and hippocampus as key epileptogenic foci, consistent with the highest-ranked computational channels.

The RMS analysis demonstrated strong bilateral activation involving orbitofrontal, hippocampal, and amygdalar regions. As shown in Figure 3.12b, stimulation of right orbitofrontal and hippocampal sites (ROF3–6, RHIP5–6) produced widespread responses across both hemispheres, indicating robust interregional connectivity. High RMS amplitudes were also observed during stimulation of both left and right amygdalar contacts (LAMI1–2, RAMI1–2), highlighting dense limbic interactions. These findings suggest that the frontal and limbic structures form an integrated epileptogenic network, supporting bilateral propagation pathways even when the primary seizure focus appears lateralized.

In conclusion, the clinical and computational findings are fully aligned, both confirming the right temporal lobe as the dominant SOZ.

3.4 *Patient* 4 *Results*

3.4.1 Connectivity Analysis Outcomes

Patient 4 (see Table 2.1) had a total of 48 channels, of which 4 were stimulated with an intensity of 10 mA (see Figure3.10). The results for this patient are presented below:

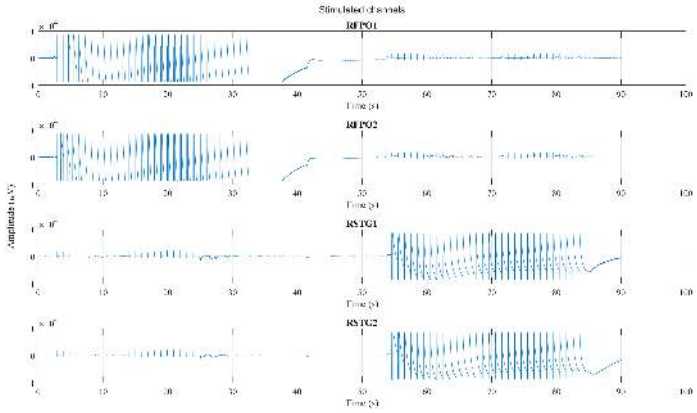

Figure 3.10. All stimulated channels for patient 4.

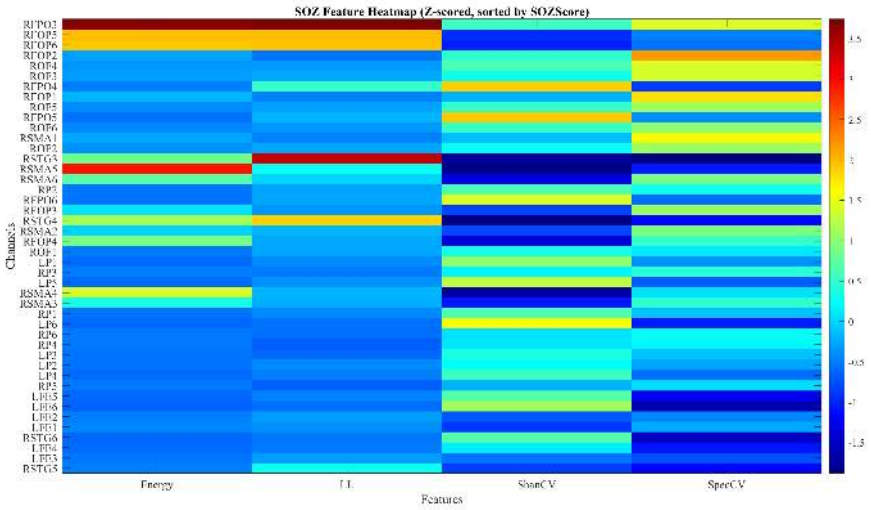

Figure 3.11. Z-score heatmap of feature extractions from non-stimulated channels in Patient 4.

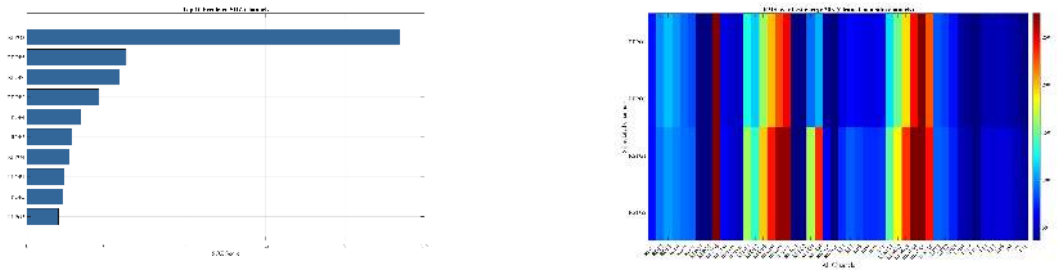

(a) **(b)**

Figure 3.12. (a) Top 10 candidate SOZ channels identified through feature extraction. (b) RMS connectivity among the regions.

3.4.2 Evaluation and Alignment of Methods

In this patient, the clinical report documented 18 seizures with identical semiology and electrophysiological onsets arising from the ROF, RFOP, and RSMA regions. Interictally, highly active independent foci were localized within RFOP and RSMA, while ROF exhibited pronounced hypersynchronous activity. The feature-based SOZ prediction model identified the top 10 candidate channels, mainly within the right fronto-opercular and orbitofrontal regions. As shown in Figure 3.12a, RFPO3 had the highest SOZ score, followed by RFOP5, RFOP6, and ROF3–4, indicating strong involvement of the lateral frontal network. The clustering of high-scoring channels in these areas suggests a focal epileptogenic zone centered on the RFPO–RFOP–ROF regions.

The RMS analysis (see Figure 3.12b) revealed the highest signal amplitudes within the right fronto-opercular (RFPO) and orbitofrontal (RFOP) regions, particularly during stimulation of nearby contacts. These areas exhibited strong local and network-level activation, indicating elevated cortical excitability. In contrast, the RSMA region showed comparatively lower RMS responses, suggesting limited direct engagement during stimulation. When integrated with the feature-based SOZ predictions, which also highlighted RFPO3, RFOP5–6, and ROF3–4 as leading candidates, the RMS results demonstrate partial alignment with the clinical seizure onset localization reported in the ROF, RFOP, and RSMA regions. Both analytical methods consistently emphasize the RFPO–RFOP–ROF territories, confirming their central role within the epileptogenic network, while the relatively lower RMS activity in RSMA indicates that mesial regions were less prominently

represented. Overall, the combined results suggest a partially aligned correspondence, with strong agreement in lateral frontal areas but weaker expression in mesial components of the clinically defined seizure onset zone.

3.5 *Patient 5 Results*

3.5.1 Connectivity Analysis Outcomes

Patient 5 (see Table 2.1) had a total of 76 channels, of which 10 were stimulated with an intensity of 10 mA (see Figure 3.13). The results for this patient are presented below:

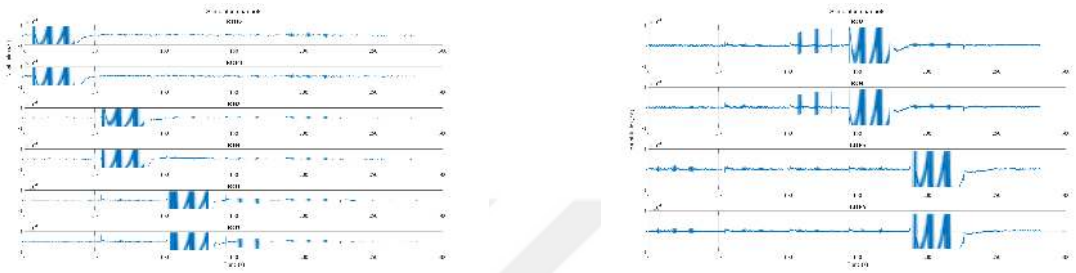

Figure 3.13. All stimulated channels for patient 5.

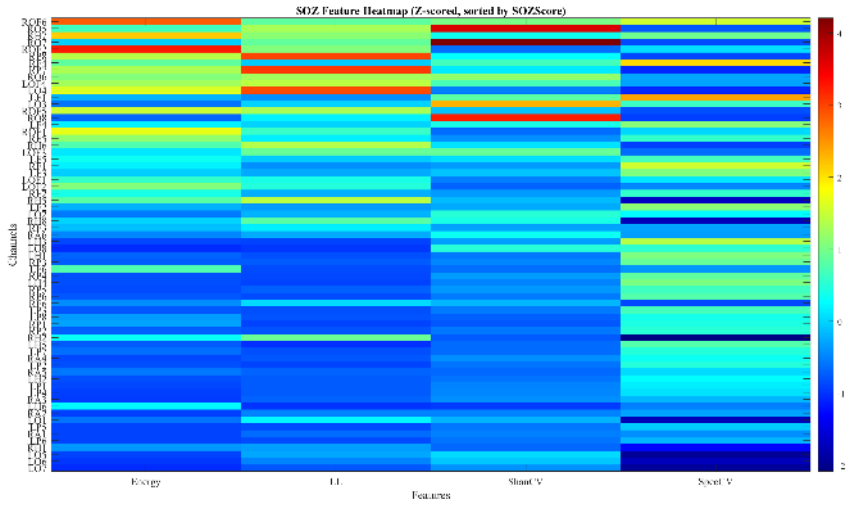

Figure 3.14. Z-score heatmap of feature extractions from non-stimulated channels in Patient 5.

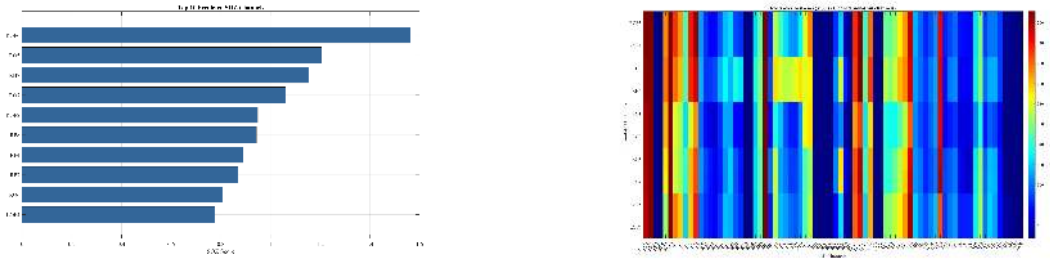

(a) **(b)**

Figure 3.15. (a) Top 10 SOZ candidate channels based on feature extraction. (b) RMS connectivity among the regions.

3.5.2 Evaluation and Alignment of Methods

Clinical monitoring documented two distinct patterns of seizure onset. Three seizures originated in the right frontotemporal region, accompanied by mild frontocentral disorganization and intermittent rhythmic delta activity (FIRDA). An additional six seizures were recorded, including one during cortical stimulation: two arose from the right hippocampus, one from the right amygdala, one from the left hippocampus (during stimulation), and two from the right occipital lobe. Interictally, marked hypersynchrony was observed in the right hippocampal contacts (1–4). Collectively, these findings define a complex epileptogenic network involving the frontotemporal, hippocampal/amygdalar, and occipital regions.

Signal processing analysis was consistent with these clinical observations. Feature extraction identified the top 10 SOZ candidate channels, including ROF6, RO5, ROF2, and RH7 (see Figure 3.15a), highlighting right frontotemporal and hippocampal involvement in agreement with the clinical seizure onsets.

The RMS analysis (Figure 3.15b) illustrates how different cortical regions responded to electrical stimulation over a 30-second high-energy window. The strongest RMS amplitudes were observed following stimulation of the right orbitofrontal (ROF3–ROF4) and right hippocampal (RH3–RH4) contacts, indicating heightened local excitability and strong network engagement within these regions. Moderate responses were also seen across the right occipital (RO1–RO4) and left orbitofrontal (LOF5–LOF6) sites, suggesting bilateral but asymmetric propagation of activity. The pattern shows that stimulation within

the right frontal and hippocampal zones elicited broad responses across temporal–occipital regions, reflecting an interconnected network rather than isolated activation. The presence of high RMS values in both hemispheres implies cross-hemispheric communication but with dominant right-hemisphere activation, consistent with right-sided network involvement. Overall, the RMS map suggests that the right orbitofrontal–hippocampal circuitry acts as a key hub for excitability and network propagation in this patient.

In conclusion, the clinical and computational findings are fully aligned, both converging on a right-dominant epileptogenic network encompassing the frontotemporal, hippocampal, and occipital regions, confirming the robustness of the multimodal analytical approach.

3.6 *Patient 6 Results*

3.6.1 Connectivity Analysis Outcomes

Patient 6 (see Table 2.1) had a total of 66 channels, of which 6 were stimulated with an intensity of 10 mA (see Figure 3.16). The results for this patient are presented below:

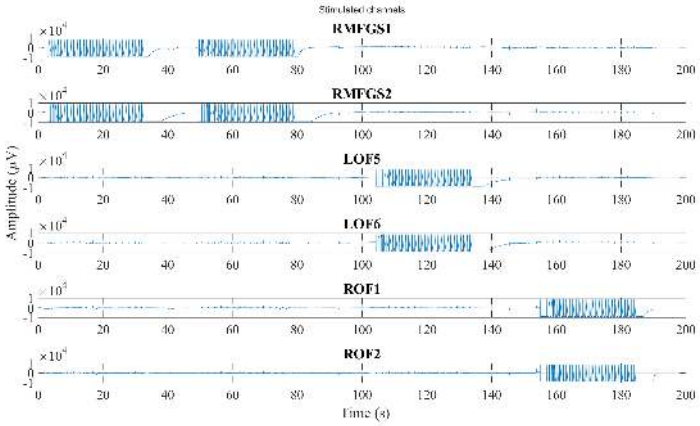

Figure 3.16. All stimulated channels for patient 6.

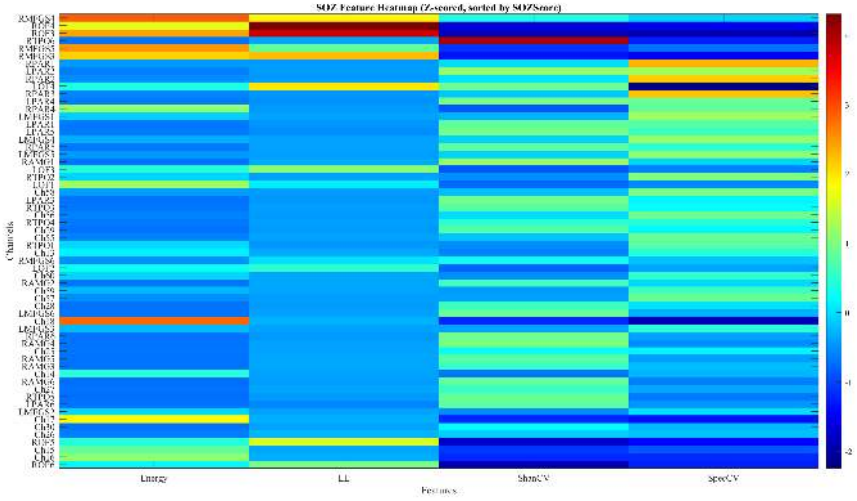

Figure 3.17. Z-score heatmap of feature extractions from non-stimulated channels in Patient 6.

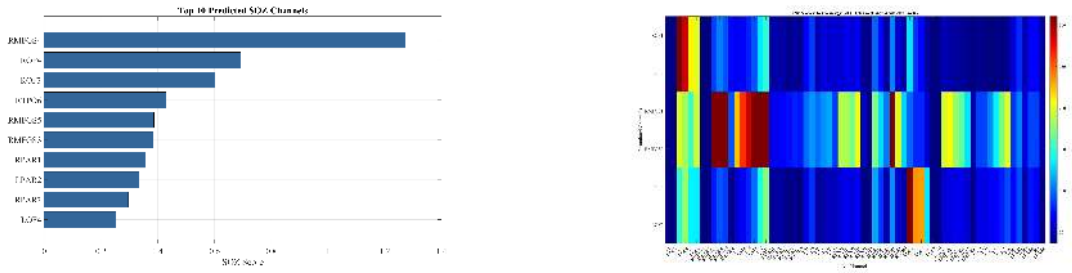

(a) **(b)**

Figure 3.18. (a) Top 10 SOZ candidate channels based on feature extraction. (b) RMS connectivity among the regions.

3.6.2 Evaluation and Alignment of Methods

Clinical monitoring identified a total of 13 seizures, with a marked predominance in the right orbitofrontal (ROF) region, where nine seizures originated, including two elicited during cortical stimulation. Additional seizures arose from the left superior midfrontal gyrus (2), right parietal cortex (1), and temporoparietooccipital region (1). Interictal recordings revealed frequent epileptiform discharges within the ROF cortex, accompanied by multiple independent foci and mild parietal disorganization. Collectively, these findings delineate the ROF cortex as the dominant epileptogenic zone within a broader frontoparietal network.

Feature-based SOZ scoring (Figure 3.18a) identified RMFGS4, ROF4, and ROF3 as leading candidate channels. In addition, the most prominent RMS elevations are seen during stimulation of the right middle frontal gyrus (see Figure 3.18b) (RMFGS1–RMFGS2) and right orbitofrontal (ROF1–ROF2) sites, indicated by strong red-to-yellow bands. These findings suggest that the right frontal regions exhibit the highest local excitability and strongest network engagement. The LOF5–LOF6 stimulations on the left side produced moderate, spatially restricted RMS increases, indicating more localized and less widespread responses. The distribution of RMS amplitudes across both hemispheres reveals bilateral activation with right-hemisphere predominance, consistent with stronger connectivity and excitability within right frontal networks. The propagation of high RMS activity from RMFGS and ROF stimulation sites into neighboring frontal and parietal channels further supports the presence of a functionally integrated frontoparietal network.

Overall, the clinical and computational results are fully aligned, converging on the right orbitofrontal and middle frontal gyri as the principal epileptogenic hubs within a right-lateralized frontoparietal network.

3.7 *Patient 7 Results*

3.7.1 Connectivity Analysis Outcomes

Patient 7 (see Table 2.1) had a total of 48 channels, 10 of which were stimulated at an intensity of 10 mA. To avoid redundancy, we do not present the plots of the stimulated signals and instead focus on the results. The findings for this patient are summarized below:

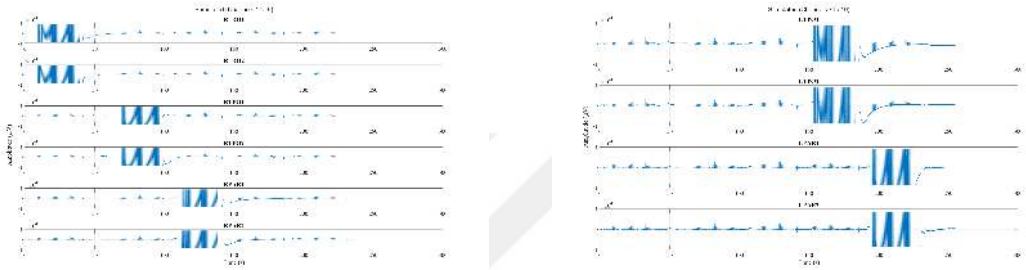

(a) **(b)**

All stimulated channels for patient 6.

Figure 3.19. All stimulated channels for patient 7.

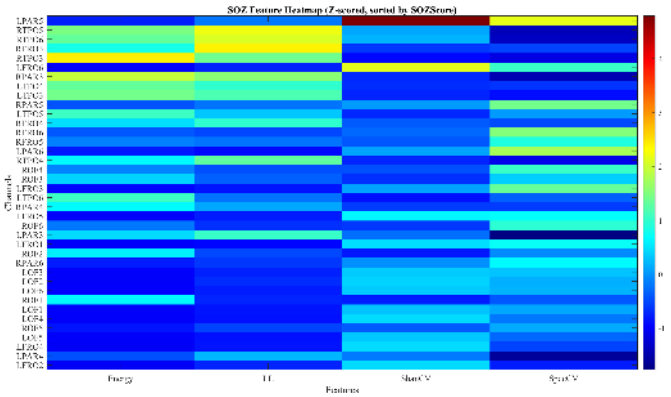

Figure 3.20. Z-score heatmap of feature extractions from non-stimulated channels in Patient 7.

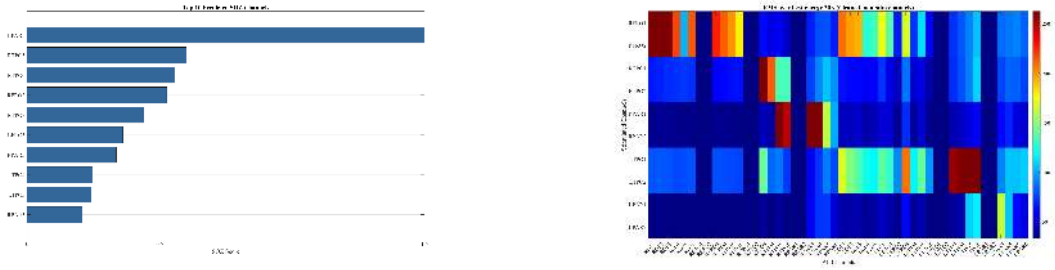

(a) **(b)**

Figure 3.21. (a) Top 10 SOZ candidate channels based on feature extraction from non-stimulated channels. (b) RMS connectivity among the regions.

3.7.2 Evaluation and Alignment of Methods

The clinical observations and signal processing outcomes reveal areas of agreement as well as differences. Clinically, the seizures were reported to arise bilaterally from posterior regions, with interictal abnormalities showing disorganization and hypersynchrony in the parieto-occipital areas. This description emphasizes the bilateral and diffuse nature of the epileptogenic process, without clear lateralization. Our signal processing results (see Figure 3.21a) similarly suggest a broad bilateral involvement, particularly highlighting both right and left parietal-occipital channels (LPAR5, RTPO5, RTPO6).

The RMS heatmap (Figure 3.21b) shows the spatial distribution of response amplitudes across all channels during the 30-second period of maximal energy, excluding the stimulated contacts. The strongest RMS elevations were observed during stimulation of the right frontoorbital (RFRO1–RFRO2) and right parietal (RPAR1–RPAR2) sites, as indicated by the prominent red-to-yellow intensity bands. These findings suggest that both right frontal and right parietal regions demonstrate high cortical excitability and strong local network engagement. Moderate responses were also seen in right temporo-parietal (RTPO2–RTPO4) and left temporo-parietal (LTPO4–LTPO5) channels, suggesting bilateral but asymmetrical propagation, with dominant activity on the right hemisphere. The relatively lower RMS amplitudes in left frontal and parietal regions indicate more localized and less extensive activation. Overall, the pattern reflects a right-lateralized functional network with strong coupling between frontal, parietal, and temporo-parietal regions, supporting the presence of an interconnected right hemispheric network likely

contributing to seizure onset and propagation.

In conclusion, the clinical and computational results are partially aligned, as both identify a bilateral, posteriorly distributed epileptogenic network involving the parieto-occipital regions without clear hemispheric dominance.

3.8 *Patient* 8 *Results*

3.8.1 Connectivity Analysis Outcomes

Patient 8 (see Table 2.1) had a total of 76 channels, 8 of which were stimulated at an intensity of 15 mA (see Figure 3.22). The findings for this patient are summarized below:

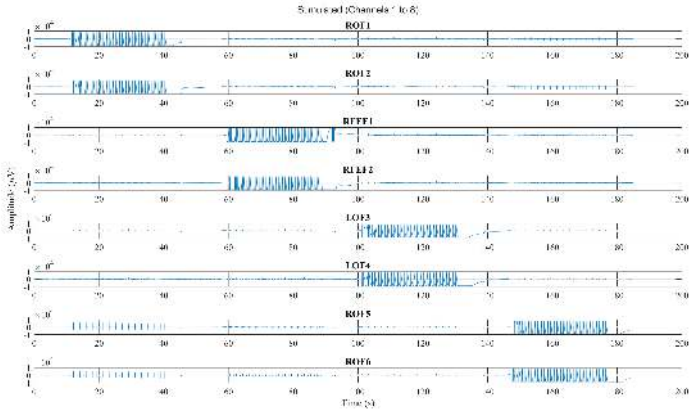

Figure 3.22. All stimulated channels for patient 8.

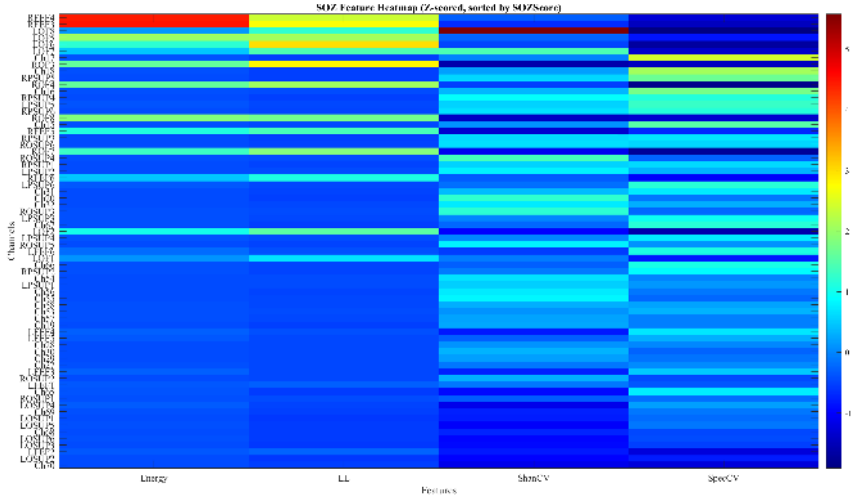

Figure 3.23. Z-score heatmap of feature extractions from non-stimulated channels in Patient 8.

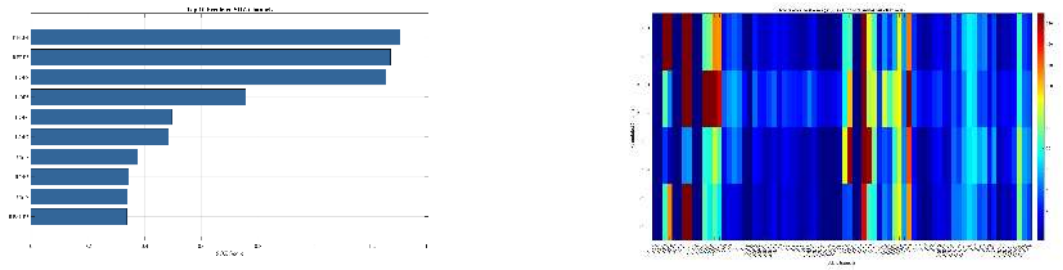

(a) **(b)**

Figure 3.24. (a) Top 10 SOZ candidate channels based on feature extraction. (b) RMS connectivity among the regions.

3.8.2 Evaluation and Alignment of Methods

The clinical findings identified seizure onset most frequently in the right frontal eye field, with additional involvement of the right superior parietal, right inferior occipital, and left orbitofrontal regions. Less frequent foci included the right orbitofrontal, right inferior parietal, and left frontal eye areas, pointing overall to a predominantly right hemispheric epileptogenic network with secondary left frontal contributions.

The signal processing analysis closely reflected these observations. The top predicted SOZ channels included RFEF3 and RFEF4, corresponding to the right frontal eye field, as well as LOF5–LOF8 and ROF3, which aligned with left orbitofrontal and right orbitofrontal involvement (see Figure 3.24a). This overlap indicates strong agreement between the clinically observed seizure onset regions and computational predictions, particularly within the frontal and parietal networks.

The RMS heatmap (Figure 3.24b) illustrates the distribution of response amplitudes across all recording channels during the 30-second high-energy window, excluding stimulated contacts. The strongest RMS activity was observed following stimulation of the right orbitofrontal (ROF1–ROF2) and right frontal eye field (RFEF1–RFEF2) sites, as shown by the distinct red and yellow intensity bands. These findings indicate marked excitability and strong local network coupling within the right frontal cortex, particularly along the orbitofrontal–frontal eye field axis. Moderate activity was also noted in left orbitofrontal channels (LOF3–LOF4), suggesting bilateral but asymmetrical activation, with the right hemisphere showing clear dominance. The propagation of high RMS responses from right

frontal to left frontal and occipital channels reflects cross-hemispheric connectivity and supports the presence of a functionally integrated bilateral frontal network. Overall, the RMS pattern points to the right frontal regions—especially the orbitofrontal and frontal eye field areas—as principal hubs of excitability and network propagation, consistent with a right-lateralized cortical activation profile.

In conclusion, the clinical, feature-based, and RMS findings are fully aligned, all indicating a right-hemispheric dominant, bilaterally connected epileptic network centered on the frontal eye field and orbitofrontal regions.

3.9 *Patient 9 Results*

3.9.1 Connectivity Analysis Outcomes

Patient 9 (see Table 2.1) had a total of 72 channels, 8 of which were stimulated at an intensity of 10 mA (see Figure 3.25). The findings for this patient are summarized below:

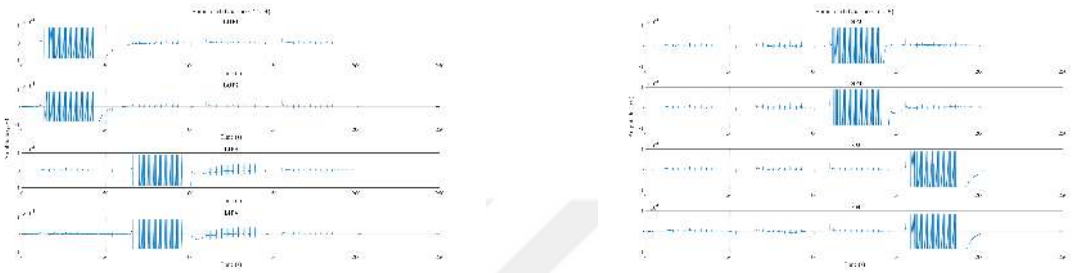

(a) **(b)**

Figure 3.25. Stimulated channels in patient 2 over 350 seconds.

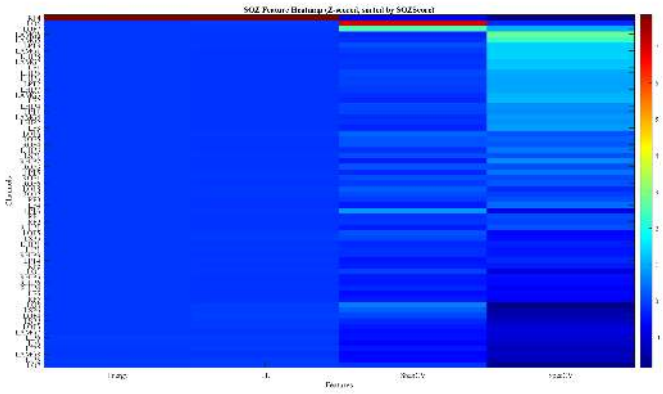

Figure 3.26. Z-score heatmap of feature extractions from non-stimulated channels in Patient 6.

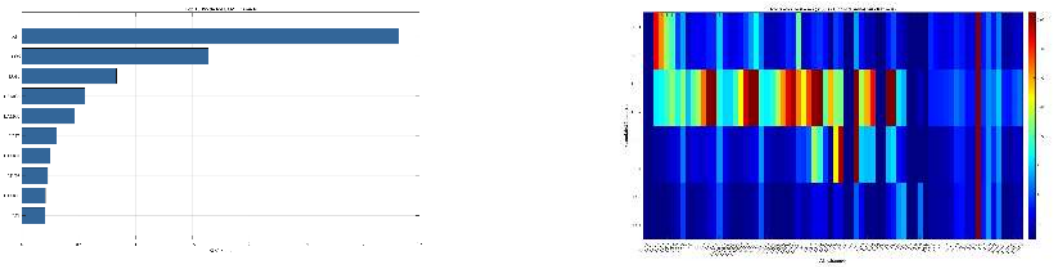

(a) **(b)**

Figure 3.27. (a) Top 10 SOZ candidate channels based on feature extraction from non-stimulated channels. (b) RMS connectivity among the regions.

3.9.2 Evaluation and Alignment of Methods

The clinical evaluation documented five seizures, most originating from the left fronto-centropemporal region, with one beginning in the posterior left hemisphere. Seizure onset clinically preceded electrophysiological onset, and temporal asynchrony was observed in three seizures. Interictal abnormalities included disorganization and hypersynchrony in the posterior left hemisphere, alongside frontal hypersynchrony, pointing to a complex but predominantly left-hemispheric epileptogenic network involving both frontal and posterior regions.

The results of signal processing highlighted RF4 as the highest ranked SOZ channel, followed by LO6 and LOF7, with several additional left hemispheric sites (LAMG, LHIP, LPT3) among the top ten (see Figure 3.27a). Importantly, LPT3 corresponded closely to the clinically observed posterior onset zone. Although the computational analysis broadly aligned with the focus of the left hemispheric region, the identification of RF4 as the leading channel introduced a partial discrepancy, as right frontal involvement was not emphasized in the clinical evaluation.

The RMS heatmap (Figure 3.27b) depicts the spatial distribution of cortical responses during the high-energy 30-second window, with stimulation applied to left-hemispheric sites. The most prominent RMS activity is observed following stimulation of the left inferior parietal (LIP3–LIP4) and left orbitofrontal (LOF1–LOF2) channels, shown by the distinct red and yellow intensity zones. This pattern indicates strong local excitability and dense intrahemispheric connectivity within the left frontoparietal network. The high-amplitude responses in these regions suggest that both the left parietal and orbitofrontal cortices are key functional hubs within this network.

Moderate propagation of RMS activity is seen across adjacent left parietal (LSP3–LSP4) and left occipital (LO3–LO4) sites, implying posterior spread of activation within the same hemisphere. In contrast, right-hemispheric channels show comparatively low responses, indicating limited cross-hemispheric propagation. Overall, the pattern reveals that stimulation in left parietal and orbitofrontal regions primarily drives local and anterior–posterior cortical engagement within the left hemisphere, consistent with a left-dominant excitability

network.

In conclusion, the alignment between clinical and computational findings is partial but strong. Both clinical and RMS analyses consistently identify a left-dominant frontoparietal network, whereas the feature-based SOZ results introduce a minor right-frontal deviation (RF4). Hence, the findings are partially aligned, with clear convergence on left-hemispheric dominance and posterior–frontal network involvement.

3.10 *Patient* 10 *Results*

3.10.1 Connectivity Analysis Outcomes

Patient 10 (see Table 2.1) had a total of 80 channels, 10 of which were stimulated at an intensity of 15 mA (see Figure 3.28). The findings for this patient are summarized below:

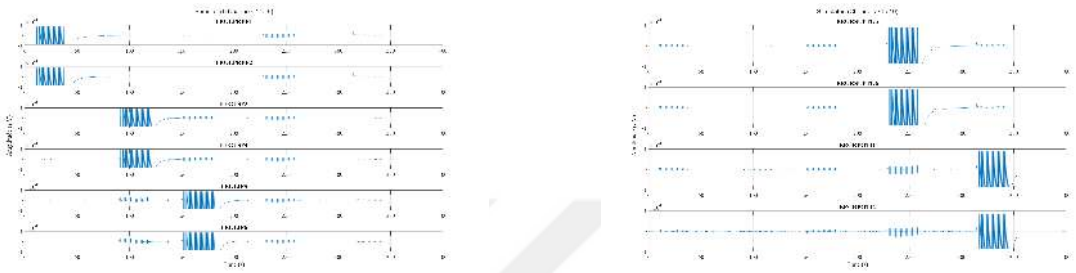

(a) **(b)**

Figure 3.28. Stimulated channels in patient 10 over 350 seconds.

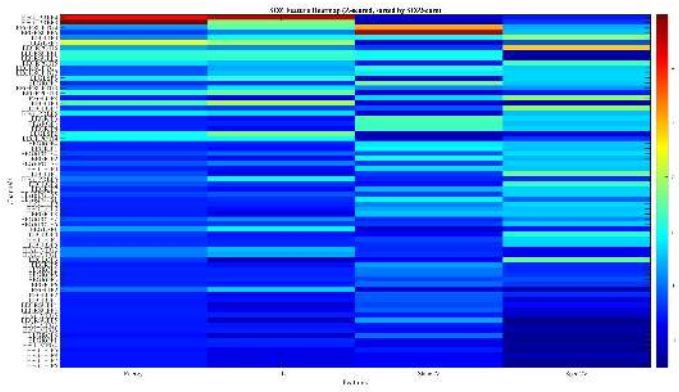

Figure 3.29. Z-score heatmap of feature extractions from non-stimulated channels in Patient 10.

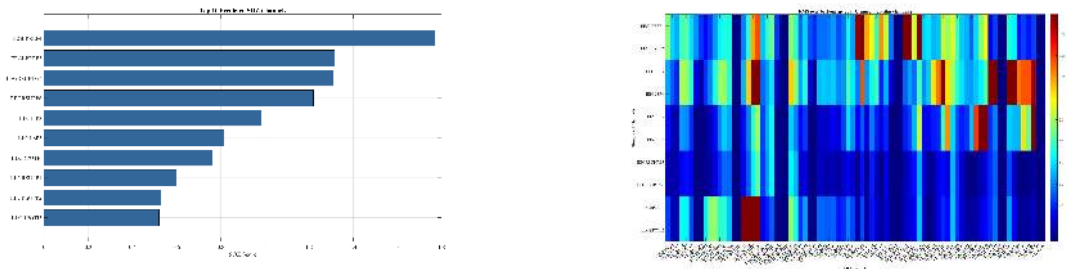

(a) **(b)**

Figure 3.30. (a) Top 10 SOZ candidate channels based on feature extraction. (b) Maximum cross-correlations between the stimulated channels and all available channel.

3.10.2 Evaluation and Alignment of Methods

The clinical and electrophysiological findings indicated seizure onset in the right orbitofrontal region, with high-frequency oscillation analysis pointing to the right superior temporal gyrus as the likely origin. Interictal abnormalities revealed additional hypersynchrony in the right inferior parietal, right posterior temporal, and left hippocampal contacts, suggesting a broader network-level involvement but with a consistent emphasis on right-sided temporal and orbitofrontal regions.

Signal processing results placed EEGLPREF4, EEGLPREF3, and EEGRSUPTG4 among the highest-ranked SOZ channels represented in Fig3.30a. In addition, the RMS heatmap (Figure 3.30b) displays that the most prominent responses occur during stimulation of left parietal and prefrontal contacts—particularly EEGLSP3–EEGLSP4 and EEGLP5–EEGLP6—suggesting robust intrahemispheric connectivity within the left parietal–frontal axis. These regions show tightly coupled local activity, reflecting a strong functional network within the left hemisphere.

Additionally, moderate activation is observed in the right superior temporal and posterior temporal regions (EEGRSUPTG5–EEGRSUPTG6, EEGRPOT11–EEGRPOT12), indicating bilateral but asymmetric propagation, with weaker right-sided involvement. The right hemisphere activity likely represents secondary spread or interhemispheric connectivity rather than primary network activation. Overall, this pattern suggests that stimulation of left frontal and parietal contacts drives the strongest and most widespread cortical engagement, forming a dominant left-hemispheric excitability network with secondary right temporal propagation. This configuration supports the presence of a bilateral but left-dominant epileptogenic network.

In conclusion, The findings are partially aligned. While both analyses identify bilateral involvement and capture the right temporal regions seen clinically, the dominant hemisphere differs — the clinical data indicate right-hemisphere onset, whereas computational measures (particularly RMS) emphasize left-sided excitability.

3.11 *Patient* 11 *Results*

3.11.1 Connectivity Analysis Outcomes

Patient 11 (see Table 2.1) had a total of 112 channels, 10 of which were stimulated at an intensity of 15 mA (see Figure 3.31). The findings for this patient are summarized below:

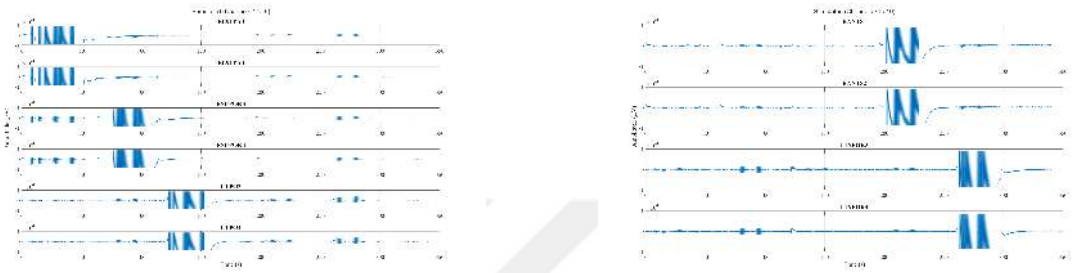

(a) **(b)**

Figure 3.31. Stimulated channels in patient 11 over 350 seconds.

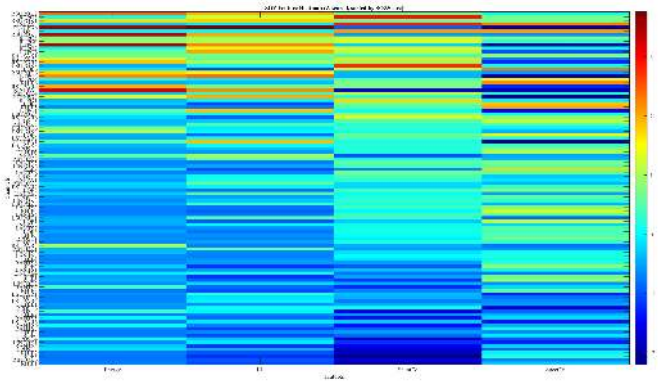

Figure 3.32. Z-score heatmap of feature extractions from non-stimulated channels in Patient 11.

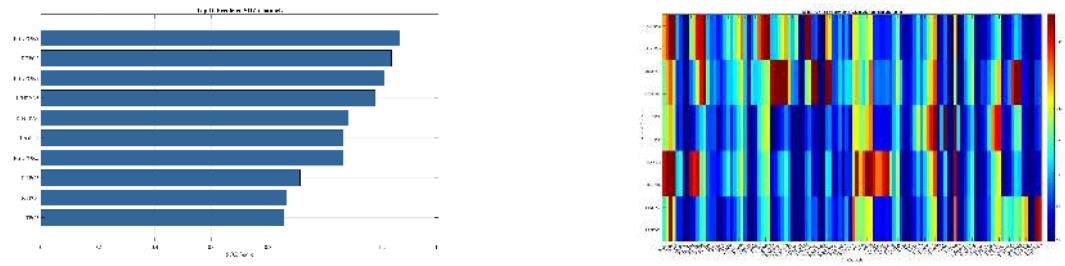

(a) **(b)**

Figure 3.33. (a) Top 10 SOZ candidate channels based on feature extraction. (b) RMS connectivity among the regions.

3.11.2 Evaluation and Alignment of Methods

Clinically, this patient demonstrated seizures originating from two distinct networks. The primary epileptogenic focus was localized to the left Temporo-Parieto-Occipital (TPO) junction, while additional seizures arose from the right orbitofrontal region. Electrophysiological recordings also revealed light-sensitive activity in the right inferior occipital and left superior occipital regions. Overall, these findings support a multifocal epileptogenic process involving both posterior cortices and orbitofrontal sites, with clear sensitivity to photic stimulation. Feature-based SOZ analysis identified RSUPOK2, RTPO3, and RSUPOK1 as the top-ranked channels (see 3.33a), along with other right parietal–temporal sites (RPOST4, RTPO5, RTPO6) and left-hemispheric contacts (LINFPA5, LTP05). This pattern indicates two main regions of susceptibility—a dominant right posterior–temporo-parietal cluster and a secondary left temporo-parietal component. The results align with the bilateral posterior cortical involvement described clinically but show a right-sided emphasis, contrasting with the clinically dominant left TPO onset.

The RMS heatmap (Figure 3.33b) further supports bilateral posterior network engagement but with distinct hemispheric differences. The strongest RMS responses were elicited by stimulation of right inferior frontal (RINFPA3–RINFPA4) and right superior parietal (RSUPOK3–RSUPOK4) sites, revealing high local excitability and strong network coupling across the right frontal–parietal cortex. In contrast, left temporo-parietal and inferior frontal regions (LTP03–LTP04, LINFOK3–LINFOK4) showed moderate activation, consistent with interhemispheric propagation rather than primary onset. The spatial distribution of RMS amplitudes highlights a dominant right-sided excitability pattern, with cross-hemispheric communication involving posterior regions bilaterally.

When integrated with the clinical findings, the computational results show partial alignment. Both the feature-based and RMS analyses confirm bilateral posterior cortical involvement and network-level coupling across occipito-parietal areas, consistent with the multifocal epileptogenic process reported clinically. However, the clinical data emphasize a left TPO onset and right orbitofrontal contribution, whereas computational metrics reveal stronger right posterior and frontal excitability, with the left hemisphere represented

less prominently. Thus, the overall interpretation indicates partial alignment — shared recognition of bilateral posterior and frontal engagement, but with differing hemispheric dominance between the clinical and computational observations.

3.12 *Patient* 12 *Results*

3.12.1 Connectivity Analysis Outcomes

Patient 12 (see Table 2.1) had a total of 120 channels, 8 of which were stimulated at an intensity of 15 mA (see Figure 3.34). The findings for this patient are summarized below:

(a) **(b)**

Figure 3.34. Stimulated channels in patient 12 over 350 seconds.

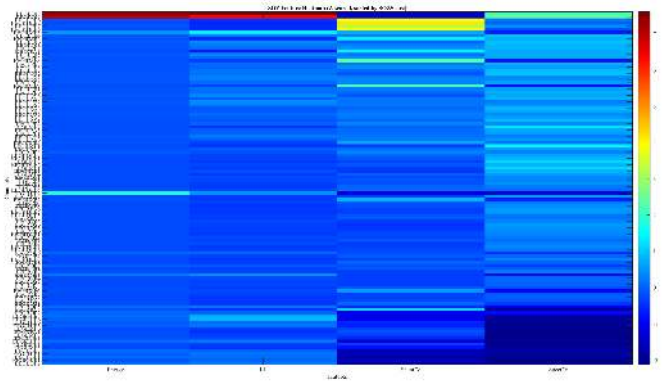

Figure 3.35. Z-score heatmap of feature extractions from non-stimulated channels in Patient 12.

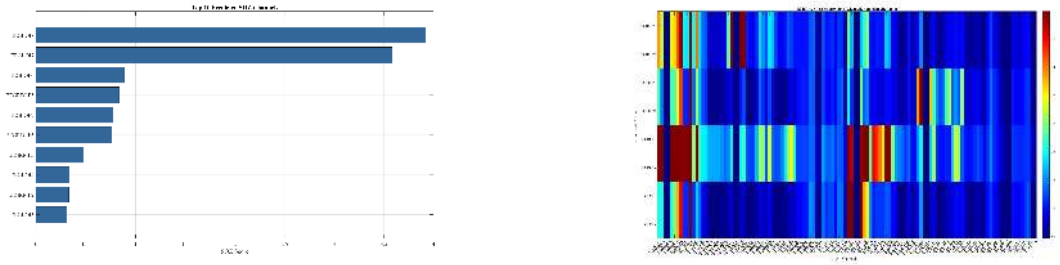

(a) **(b)**

Figure 3.36. (a) Top 10 SOZ candidate channels based on feature extraction from non-stimulated channels. (b) RMS connectivity among the regions.

3.12.2 Evaluation and Alignment of Methods

Clinically, four seizures were recorded with onset localized to the right orbitofrontal region. Interictal activity revealed independent foci in the right orbitofrontal and right mid-frontal regions. High-frequency oscillation (HFO) analysis emphasized the right mid-frontal cortex as the most prominent generator but also demonstrated additional involvement of the right anterior parietal, right orbitofrontal, left inferior occipital, left orbitofrontal, and left posterior parietal regions. Collectively, these findings describe a multifocal but frontal-dominant epileptogenic network, with bilateral parietal and occipital contributions.

As shown in Figure 3.21a, signal processing highlighted EEGLOI8 and EEGLOI7 (left orbitofrontal) as the strongest SOZ channels, along with EEGLOF6/7 (left orbitofrontal), EEGRDLF5/6 (right dorsolateral frontal), and EEGRMF3 (right mid-frontal).

The RMS heatmap (Figure 3.21b) reveals pronounced activation in both right and left orbitofrontal and hippocampal regions, shown by the red–yellow intensity bands during stimulation of EEGROF3–EEGROF4 (right orbitofrontal) and EEGLOF3–EEGLOF4 (left orbitofrontal) channels. Additionally, EEGRHIP3–EEGRHIP4 and EEGLHIP3–EEGLHIP4 exhibit moderate-to-strong responses, suggesting network coupling between frontal and mesial temporal structures bilaterally. The pattern indicates bilateral but asymmetric engagement, with stronger excitability across the right orbitofrontal and hippocampal sites, and secondary activation in left orbitofrontal regions. Overall, the heatmap reflects a frontal-dominant excitability profile with temporal connectivity, consistent with a multifocal but interconnected network.

In conclusion, the clinical, feature-based, and RMS analyses demonstrate strong alignment, all converging on a frontal-dominant epileptogenic network centered in the right orbitofrontal and mid-frontal cortex, with additional bilateral orbitofrontal participation and temporal propagation. The RMS map reinforces this by showing high excitability within the orbitofrontal network (right > left) and secondary engagement of hippocampal regions, likely reflecting downstream connectivity. Minor differences—such as a slightly stronger left orbitofrontal emphasis in the computational results—represent natural asymmetry rather than a true mismatch. Overall, the findings are fully aligned, confirming a bilaterally interconnected but right-dominant frontal network as the core of epileptogenic activity.

3.13 *Overall Evaluation of Results*

Across all twelve cases, the alignment between clinical evaluations and computational analyses (feature-based SOZ prediction and RMS connectivity mapping) demonstrates a high degree of convergence, with partial or full correspondence observed in over **80**% of patients. The multimodal integration of clinical seizure data, quantitative signal analysis, and RMS-based functional mapping reveals consistent patterns: seizures rarely arise from strictly localized foci but instead from distributed, interconnected cortical–subcortical networks with variable lateralization.

Patterns of Alignment Five patients (Cases 3, 5, 6, 8, and 12) showed full alignment, where both clinical and computational methods independently identified the same dominant epileptogenic zones. These cases frequently involved well-defined, focal onsets—particularly within right mesial temporal or frontal regions—where concordant SOZ predictions and RMS activation maps reinforced the same network hubs. The coherence of findings in these cases supports the reliability of quantitative modeling in confirming clinical impressions and delineating propagation pathways.

Other six patients (Cases 1, 2, 4, 9, 10, and 11) demonstrated partial alignment, marked by agreement on general network topology but divergence in hemispheric dominance or secondary propagation territories. In these cases, the clinical evaluations typically empha-

sized a focal or lateralized onset (e.g., right temporal or left frontal), while computational methods revealed broader or contralateral network participation—often implicating opercular, orbitofrontal, or parietal regions. These differences emphasize that computational analyses are highly sensitive to detecting widespread excitability patterns that can emerge before or alongside clinically observable seizure activity. Importantly, these discrepancies should not be interpreted as contradictions but rather as evidence of subthreshold network co-activation beyond the primary clinical focus.

Only one case (Case 7) exhibited bilateral equivalence, with both approaches identifying diffuse posterior parieto-occipital involvement lacking clear lateralization. This pattern underscores the challenge of defining a single SOZ in highly symmetrical or multifocal epileptic networks and further validates the computational tools' ability to capture distributed activity consistent with clinical interpretation.

Network-Level Insights Across patients, two recurring network archetypes emerged:

Frontal–Opercular Circuits: Frequently implicated in both clinical and RMS analyses, these regions (RFOP, ROF, LFO, and opercular zones) consistently exhibited high RMS amplitudes and strong interhemispheric coupling, positioning them as network hubs for seizure propagation and bilateral communication.

Temporal–Limbic Pathways: Right mesial temporal structures (amygdala and hippocampus) were repeatedly identified as SOZ centers in both modalities, often with secondary orbitofrontal or parietal connectivity, reflecting the canonical limbic seizure network. Additionally, posterior parietal–occipital networks appeared prominently in patients with bilateral or diffuse epilepsies, emphasizing their role in multisite synchronization and photic sensitivity.

Interpretation of Divergences Discrepancies between clinical and computational outcomes primarily reflect differences in methodological focus. Clinical evaluations emphasize seizure onset zones derived from behavioral and electrophysiological correlates, while computational models capture high synchronization and network excitability patterns that may underlie or anticipate clinical onset. RMS connectivity maps, by quantifying cortical responsiveness, often reveal functionally connected but subclinical territories that

contribute to seizure generalization. Therefore, apparent mismatches—such as left-sided RMS dominance in a right-onset seizure—likely represent complementary dimensions of the same underlying epileptogenic network.

Clinical Implications The recurring identification of widespread, frequently bilateral networks across several patients questions the traditional view of epilepsy as a purely focal disorder and highlights the importance of adopting network-oriented approaches for surgical and neuromodulation interventions. Integrating computational modeling and RMS connectivity analyses into presurgical planning could refine SOZ delineation, identify critical propagation hubs, and reduce the risk of incomplete resection. Moreover, the strong agreement observed across modalities supports the clinical value of data-driven SOZ prediction as a complementary tool alongside expert electrophysiological evaluation.

Taken together, the multimodal analyses provide convergent evidence that epileptogenic activity arises from interconnected cortical–subcortical networks with variable lateralization and regional dominance. While clinical findings define the primary seizure onset zones, computational analyses—particularly RMS mapping—extend this understanding to encompass broader functional architectures. The resulting synthesis underscores a key paradigm shift in epilepsy research and treatment: from focal localization toward network-informed precision neuromodulation and surgical targeting.

CHAPTER 4

CONCLUSION AND LIMITATIONS

In this study, raw SEEG-derived CCEPs signals were processed using a systematic preprocessing and feature-extraction pipeline to identify SOZ localizations in DRE patients. To achieve this, the first step involved cleaning the signals to remove noise and artifacts. A bandpass filter (1–1000 Hz) and a 50 Hz notch filter were applied to suppress slow drifts and powerline interference, thereby ensuring that subsequent features captured physiologically relevant activity. For non-stimulated channels, a dedicated artifact-removal procedure was employed: stimulation-related artifacts—characterized by sharp periodic peaks—were detected and corrected within a ±10 ms window using linear and nearest-neighbor interpolation. This step was essential to minimize stimulation-related distortions in correlation analyses.

Afterward, for non-stimulated channels, a sliding 30-second epoching approach was employed, using energy and line length as discriminative features to identify the most representative segments. Within these epochs, short-window (0.98 s) measures of Shannon entropy and SE were extracted, providing complementary descriptors of signal complexity and epileptogenic behavior. Feature values were standardized (z-scored) and integrated into a composite SOZ score, which enabled objective ranking of channels. The highest-ranked contacts were then compared against stimulation-cleaned cross-correlation matrices, yielding a dual filter that prioritized channels demonstrating both abnormal local features and strong network connectivity to the stimulated sites.

Finally, Root Mean Square was computed for the cleaned and interpolated artifact

free non-stimulated channels to analize the connections between the regions. Overall, computational SOZ analysis demonstrated close alignment with clinical findings over **80**%. However, several limitations should be considered when interpreting these findings:

- **Sample Size:** The study included only twelve patients with DRE, which limits generalizability. Although the dataset was rich in multimodal detail, statistical power remained constrained, and validation in larger cohorts is warranted.
- **Partial Clinical Alignment:** In 6 of 12 cases, computational and clinical interpretations demonstrated only partial overlap. This likely reflects the inherent complexity of distributed and bilateral epileptogenic networks rather than methodological error, underscoring the challenge of achieving perfect concordance between computational and clinical assessments.
- **Feature Extraction Limitation:** Feature extraction was restricted to non-stimulated channels. If stimulated contacts were part of the true SOZ, they would have been excluded, potentially underrepresenting critical regions.
- **Electrode Coverage Constraints:** Implantation strategies inherently limited spatial sampling. Some regions of interest were not directly recorded, restricting the capacity of computational methods to fully characterize seizure networks.
- **Temporal Sampling:** Analyses were based on relatively short recording epochs based on each patient available data duration (e.g., 200 seconds). Given that seizure dynamics evolve over longer timescales, these snapshots may not fully capture SOZ variability.

Future research can address these limitations and extend the present findings through several directions:

- **Expanded Cohorts:** Replicating the analysis in larger and more diverse patient populations will strengthen statistical validation and help assess generalizability across epilepsy subtypes.

- **Integration of Stimulated Channels:** Future pipelines should incorporate stimulated contacts into feature extraction to avoid systematic exclusion of potential SOZ candidate regions. A practical approach would be to remove only the stimulation interval from the affected channels while preserving the remaining data. For instance, if a stimulation pair such as LOF5–LOF6 is active between 20–50 seconds of the recording, the corresponding 30-second segment can be excised, and the pre- and post-stimulation portions concatenated into a continuous trace. This strategy retains the majority of the physiological signal while eliminating stimulation artifacts, enabling standard feature extraction to be performed on stimulated channels without introducing bias or distortion.

- **Multimodal Integration:** Combining computational SOZ identification with imaging modalities (MRI, PET, fMRI) or high-frequency oscillation analysis could enhance localization and mitigate the biases of any single modality.

- **Clinical Translation:** Prospective studies are needed to evaluate how correlation-refined targets influence surgical decision-making and patient outcomes. Trials directly comparing resections guided by these computational markers versus standard clinical practice would provide definitive evidence of clinical utility.

BIBLIOGRAPHY

Aarabi, A., Fazel-Rezai, R., and Aghakhani, Y. (2009). A fuzzy rule-based system for epileptic seizure detection in intracranial eeg. *Clinical Neurophysiology*, 120(9):1648–1657.

Akkol, S., Kucyi, A., Hu, W., Zhao, B., Zhang, C., Sava-Segal, C., Liu, S., Razavi, B., Zhang, J., Zhang, K., et al. (2021). Intracranial electroencephalography reveals selective responses to cognitive stimuli in the periventricular heterotopias. *Journal of Neuroscience*, 41(17):3870–3878.

Al-Sadek, T., Wadhwa, A., Wadhwa, M., Warren, A. E., and Rolston, J. D. (2025). Methodologies to detect cortico-cortical evoked potentials: a systematic review. *Frontiers in Human Neuroscience*, 19:1636115.

Alarcón, G., Jiménez-Jiménez, D., Valentín, A., and Martín-López, D. (2018). Characterizing eeg cortical dynamics and connectivity with responses to single pulse electrical stimulation (spes). *International journal of neural systems*, 28(06):1750057.

Angulo-Ruiz, B. Y., Munoz, V., Rodríguez-Martínez, E. I., Cabello-Navarro, C., and Gomez, C. M. (2023). Multiscale entropy of adhd children during resting state condition. *Cognitive neurodynamics*, 17(4):869–891.

Bartolomei, F., Lagarde, S., Wendling, F., McGonigal, A., Jirsa, V., Guye, M., and Bénar, C. (2017). Defining epileptogenic networks: contribution of seeg and signal analysis. *Epilepsia*, 58(7):1131–1147.

Boonyakitanont, P., Lek-Uthai, A., Chomtho, K., and Songsiri, J. (2020). A review of

feature extraction and performance evaluation in epileptic seizure detection using eeg. *Biomedical Signal Processing and Control*, 57:101702.

Cornblath, E. J., Lucas, A., Armstrong, C., Greenblatt, A. S., Stein, J. M., Hadar, P. N., Raghupathi, R., Marsh, E., Litt, B., Davis, K. A., et al. (2023). Quantifying trial-by-trial variability during cortico-cortical evoked potential mapping of epileptogenic tissue. *Epilepsia*, 64(4):1021–1034.

Dionisio, S., Mayoglou, L., Cho, S.-M., Prime, D., Flanigan, P. M., Lega, B., Mosher, J., Leahy, R., Gonzalez-Martinez, J., and Nair, D. (2019). Connectivity of the human insula: A cortico-cortical evoked potential (ccep) study. *Cortex*, 120:419–442.

Enatsu, R., Gonzalez-Martinez, J., Bulacio, J., Kubota, Y., Mosher, J., Burgess, R. C., Najm, I., and Nair, D. R. (2015). Connections of the limbic network: a corticocortical evoked potentials study. *Cortex*, 62:20–33.

Engel, J., Thompson, P. M., Stern, J. M., Staba, R. J., Bragin, A., Mody, I., et al. (2013). Connectomics and epilepsy. *Current opinion in neurology*, 26(2):186–194.

Feys, O., Schuind, S., Sculier, C., Rikir, E., Legros, B., Gaspard, N., Wens, V., and De Tiège, X. (2025). Dynamics of magnetic cortico-cortical responses evoked by single-pulse electrical stimulation. *Epilepsia*, 66(2):503–517.

Helakari, H., Kananen, J., Huotari, N., Raitamaa, L., Tuovinen, T., Borchardt, V., Rasila, A., Raatikainen, V., Starck, T., Hautaniemi, T., Myllylä, T., Tervonen, O., Rytky, S., Keinänen, T., Korhonen, V., Kiviniemi, V., and Ansakorpi, H. (2019). Spectral entropy indicates electrophysiological and hemodynamic changes in drug-resistant epilepsy – a multimodal mreg study. *NeuroImage: Clinical*, 22:101763.

Howard, M. A., Volkov, I., Mirsky, R., Garell, P., Noh, M., Granner, M., Damasio, H., Steinschneider, M., Reale, R., Hind, J., et al. (2000). Auditory cortex on the human posterior superior temporal gyrus. *Journal of Comparative Neurology*, 416(1):79–92.

Hu, X., Yao, Y., Zhao, B., Wang, X., Li, Z., Hu, W., Zhang, C., and Zhang, K. (2025).

Effective connectivity predicts surgical outcomes in temporal lobe epilepsy: A seeg study. *CNS Neuroscience & Therapeutics*, 31(8):e70563.

Huang, H., Gregg, N. M., Valencia, G. O., Brinkmann, B. H., Lundstrom, B. N., Worrell, G. A., Miller, K. J., and Hermes, D. (2023). Electrical stimulation of temporal and limbic circuitry produces distinct responses in human ventral temporal cortex. *Journal of Neuroscience*, 43(24):4434–4447.

Inouye, T., Shinosaki, K., Sakamoto, H., Toi, S., Ukai, S., Iyama, A., Katsuda, Y., and Hirano, M. (1991). Quantification of eeg irregularity by use of the entropy of the power spectrum. *Electroencephalography and clinical neurophysiology*, 79(3):204–210.

Jobst, B. C., Bartolomei, F., Diehl, B., Frauscher, B., Kahane, P., Minotti, L., Sharan, A., Tardy, N., Worrell, G., and Gotman, J. (2020). Intracranial eeg in the 21st century. *Epilepsy currents*, 20(4):180–188.

Jobst, B. C. and Cascino, G. D. (2015). Resective epilepsy surgery for drug-resistant focal epilepsy: a review. *Jama*, 313(3):285–293.

Keller, C. J., Honey, C. J., Mégevand, P., Entz, L., Ulbert, I., and Mehta, A. D. (2014). Mapping human brain networks with cortico-cortical evoked potentials. *Philosophical Transactions of the Royal Society B: Biological Sciences*, 369(1653):20130528.

Kharbouch, A., Shoeb, A., Guttag, J., and Cash, S. S. (2011). An algorithm for seizure onset detection using intracranial eeg. *Epilepsy & Behavior*, 22:S29–S35.

Kirch, W., editor (2008). *z-Score*, pages 1484–1484. Springer Netherlands, Dordrecht.

Kunieda, T., Yamao, Y., Kikuchi, T., and Matsumoto, R. (2015). New approach for exploring cerebral functional connectivity: review of cortico-cortical evoked potential. *Neurologia medico-chirurgica*, 55(5):374–382.

Lemaréchal, J.-D., Jedynak, M., Trebaul, L., Boyer, A., Tadel, F., Bhattacharjee, M., Deman, P., Tuyisenge, V., Ayoubian, L., Hugues, E., et al. (2022). A brain atlas of

axonal and synaptic delays based on modelling of cortico-cortical evoked potentials. *Brain*, 145(5):1653–1667.

Levinson, L., Sun, S., Paschall, C., Perks, K., Weaver, K., Perlmutter, S., Ko, A., Ojemann, J., and Herron, J. (2024). Data processing techniques impact quantification of cortico-cortical evoked potentials. *Journal of Neuroscience Methods*, 408:110130.

Lo, Y., Hsiao, Y.-T., and Chang, F.-C. (2022). Use electroencephalogram entropy as an indicator to detect stress-induced sleep alteration. *Applied Sciences*, 12(10):4812.

Mariani, V., Sartori, I., Revay, M., Mai, R., Lizio, D., Berta, L., Rizzi, M., and Cossu, M. (2021). Intraoperative corticocortical evoked potentials for language monitoring in epilepsy surgery. *World Neurosurgery*, 151:e109–e121.

Matsumoto, R., Nair, D. R., LaPresto, E., Bingaman, W., Shibasaki, H., and Lüders, H. O. (2007). Functional connectivity in human cortical motor system: a cortico-cortical evoked potential study. *Brain*, 130(1):181–197.

Matsumoto, R., Nair, D. R., LaPresto, E., Najm, I., Bingaman, W., Shibasaki, H., and Lüders, H. O. (2004). Functional connectivity in the human language system: a cortico-cortical evoked potential study. *Brain*, 127(10):2316–2330.

Mitsuhashi, T., Sonoda, M., Iwaki, H., Luat, A. F., Sood, S., and Asano, E. (2020). Effects of depth electrode montage and single-pulse electrical stimulation sites on neuronal responses and effective connectivity. *Clinical Neurophysiology*, 131(12):2781–2792.

Mouthaan, B. E., van't Klooster, M. A., Keizer, D., Hebbink, G. J., Leijten, F. S., Ferrier, C. H., Van Putten, M. J., Zijlmans, M., and Huiskamp, G. J. (2016). Single pulse electrical stimulation to identify epileptogenic cortex: Clinical information obtained from early evoked responses. *Clinical neurophysiology*, 127(2):1088–1098.

Parker, C. S., Clayden, J. D., Cardoso, M. J., Rodionov, R., Duncan, J. S., Scott, C., Diehl, B., and Ourselin, S. (2018). Structural and effective connectivity in focal epilepsy. *NeuroImage: Clinical*, 17:943–952.

Qiang, Z., Norris, J., Cooray, G., Rosch, R., Miller, K., Hermes, D., Chari, A., and Tisdall, M. (2025). Cortico-cortical evoked potentials: Analytical techniques and emerging paradigms for epileptogenic zone localization. *Epilepsia*.

Rosenow, F. and Lüders, H. (2001). Presurgical evaluation of epilepsy. *Brain*, 124(9):1683–1700.

Saito, T., Tamura, M., Muragaki, Y., Maruyama, T., Kubota, Y., Fukuchi, S., Nitta, M., Chernov, M., Okamoto, S., Sugiyama, K., et al. (2014). Intraoperative cortico-cortical evoked potentials for the evaluation of language function during brain tumor resection: initial experience with 13 cases. *Journal of neurosurgery*, 121(4):827–838.

Sanei, S. and Chambers, J. A. (2013). *EEG signal processing*. John Wiley & Sons.

Schaworonkow, N. and Voytek, B. (2021). Enhancing oscillations in intracranial electrophysiological recordings with data-driven spatial filters. *PLoS Computational Biology*, 17(8):e1009298.

Seidel, K., Wermelinger, J., Alvarez-Abut, P., Deletis, V., Raabe, A., Zhang, D., and Schucht, P. (2024). Cortico-cortical evoked potentials of language tracts in minimally invasive glioma surgery guided by penfield stimulation. *Clinical Neurophysiology*, 161:256–267.

Shannon, C. E. (1948). A mathematical theory of communication. *The Bell system technical journal*, 27(3):379–423.

Shoeibi, A., Sadeghi, D., Moridian, P., Ghassemi, N., Heras, J., Alizadehsani, R., Khadem, A., Kong, Y., Nahavandi, S., Zhang, Y.-D., et al. (2021). Automatic diagnosis of schizophrenia in eeg signals using cnn-lstm models. *Frontiers in neuroinformatics*, 15:777977.

Singh, A. K. and Krishnan, S. (2023). Trends in eeg signal feature extraction applications. *Frontiers in artificial intelligence*, 5:1072801.

Tenev, A., Markovska-Simoska, S., Müller, A., and Mishkovski, I. (2025). Entropy, complexity, and spectral features of eeg signals in autism and typical development: a quantitative approach. *Frontiers in Psychiatry*, 16:1505297.

Thompson, B. (2004). *Exploratory and confirmatory factor analysis: Understanding concepts and applications.* American Psychological Association.

Tian, Y., Zhang, H., Xu, W., Zhang, H., Yang, L., Zheng, S., and Shi, Y. (2017). Spectral entropy can predict changes of working memory performance reduced by short-time training in the delayed-match-to-sample task. *Frontiers in human neuroscience*, 11:437.

Tomlinson, S. B., Baumgartner, M. E., Darlington, T. R., Marsh, E. D., and Kennedy, B. C. (2025). Mapping the epileptogenic brain using low-frequency stimulation: Two decades of advances and uncertainties. *Journal of Clinical Medicine*, 14(6):1956.

van't Klooster, M. A., Zijlmans, M., Leijten, F. S., Ferrier, C. H., Van Putten, M. J., and Huiskamp, G. J. (2011). Time–frequency analysis of single pulse electrical stimulation to assist delineation of epileptogenic cortex. *Brain*, 134(10):2855–2866.

Wang, F., Chen, X., and Roelfsema, P. R. (2024). Comparison of electrical microstimulation artifact removal methods for high-channel-count prostheses. *Journal of Neuroscience Methods*, 408:110169.

Welch, P. D. (1967). The use of fast fourier transform for the estimation of power spectra: A method based on time averaging over short, modified periodograms. *IEEE Transactions on Audio and Electroacoustics*, 15(2):70–73.

Widmann, A., Schröger, E., and Maess, B. (2015). Digital filter design for electrophysiological data–a practical approach. *Journal of neuroscience methods*, 250:34–46.

Wiebe, S., Blume, W. T., Girvin, J. P., and Eliasziw, M. (2001). A randomized, controlled trial of surgery for temporal-lobe epilepsy. *New England Journal of Medicine*, 345(5):311–318.

Wu, T., Kong, X., Zhong, Y., and Chen, L. (2022). Automatic detection of abnormal eeg signals using multiscale features with ensemble learning. *Frontiers in Human Neuroscience*, 16:943258.

Xie, T., Foutz, T. J., Adamek, M., Swift, J. R., Inman, C. S., Manns, J. R., Leuthardt, E. C., Willie, J. T., and Brunner, P. (2023). Single-pulse electrical stimulation artifact removal using the novel matching pursuit-based artifact reconstruction and removal method (mparrm). *Journal of Neural Engineering*, 20(6):066036.

Ye, H., Fan, Z., Li, G., Wu, Z., Hu, J., Sheng, X., Chen, L., and Zhu, X. (2022). Spontaneous state detection using time-frequency and time-domain features extracted from stereo-electroencephalography traces. *Frontiers in Neuroscience*, 16:818214.